bioRxiv preprint doi: https://doi.org/10.1101/386458; this version posted August 7, 2018. The copyright holder for this preprint (which was not certified by peer review) is the author/funder, who has granted bioRxiv a license to display the preprint in perpetuity. It is made available under aCC-BY-NC-ND 4.0 International license.

The crossover function of MutSγ is activated via Cdc7-dependent stabilization of Msh4

Authors: Wei He[1,2], H.B.D. Prasada Rao[1,2,†], Shangming Tang[1,2], Nikhil Bhagwat[1,2], Dhananjaya Kulkarni[1,2], Yunmei Ma[1], Maria A.W. Chang[1], Christie Hall[1], Junxi Wang-Bragg[1], Harrison S. Manasca[1], Christa Baker[1], Gerrik F. Verhees[1], Lepakshi Singh[3], Xiangyu Chen[4], Nancy M. Hollingsworth[4], Petr Cejka[3] and Neil Hunter [1,2,5,6]

Affiliations:

[1]Howard Hughes Medical Institute, University of California, Davis, Davis, California, USA.

[2]Department of Microbiology & Molecular Genetics, University of California, Davis, Davis, California, USA.

[3]Institute for Research in Biomedicine, Università della Svizzera italiana, Bellinzona, Switzerland.

[4]Department of Biochemistry and Cell Biology, Stony Brook University, Stony Brook, New York, United States of America.

[5]Department of Molecular & Cellular Biology, University of California, Davis, Davis, California, USA.

[6]Department of Cell Biology & Human Anatomy, University of California, Davis, Davis, California, USA.

† Current address: National Institute of Animal Biotechnology, Hyderabad, Telangana, India.

* Correspondence to: Neil Hunter, E-mail: nhunter@ucdavis.edu

bioRxiv preprint doi: https://doi.org/10.1101/386458; this version posted August 7, 2018. The copyright holder for this preprint (which was not certified by peer review) is the author/funder, who has granted bioRxiv a license to display the preprint in perpetuity. It is made available under aCC-BY-NC-ND 4.0 International license.

SUMMARY

The MutSγ complex, Msh4-Msh5, binds DNA joint-molecule (JM) intermediates during homologous recombination to promote crossing over and accurate chromosome segregation at the first division of meiosis. MutSγ facilitates the formation and biased resolution of crossover-specific JM intermediates called double Holliday junctions. Here we show that these activities are governed by regulated proteasomal degradation. MutSγ is initially inactive for crossing over due to an N-terminal degron on Msh4 that renders it unstable. Activation of MutSγ requires the Dbf4-dependent kinase, Cdc7 (DDK), which directly phosphorylates and thereby neutralizes the Msh4 degron. Phosphorylated Msh4 is chromatin bound and requires DNA strand exchange and chromosome synapsis, implying that DDK specifically targets MutSγ that has already bound nascent JMs. Our study establishes regulated protein degradation as a fundamental mechanism underlying meiotic crossover control.

bioRxiv preprint doi: https://doi.org/10.1101/386458; this version posted August 7, 2018. The copyright holder for this preprint (which was not certified by peer review) is the author/funder, who has granted bioRxiv a license to display the preprint in perpetuity. It is made available under aCC-BY-NC-ND 4.0 International license.

INTRODUCTION

Crossing over is required for the accurate segregation of homologous chromosomes (homologs) at the first division of meiosis (Hunter, 2015; Watanabe, 2012). At metaphase I, the four chromatids of a bivalent are interconnected by cohesion between sister chromatids and at least one crossover between the homologs. These connections enable stable bipolar attachment of bivalents to the meiosis-I spindle, which is a prerequisite for accurate homolog disjunction at the ensuing anaphase. Crossing over is highly regulated to ensure that homolog pairs obtain the requisite connection despite a low average number of crossovers per nucleus (Jones, 1984). Also, crossovers between a single homolog pair inhibit one another such that multiple events tend to be widely and evenly spaced. Together, these crossover assurance and crossover interference processes dictate the range of crossover numbers per nucleus. In *C. elegans*, absolute interference, effective along the entire lengths of all chromosomes, minimizes crossover numbers to one per chromosome (Hillers and Villeneuve, 2003). More typically, crossovers average around one per chromosome arm, but smaller chromosomes will often obtain only a single exchange. Suboptimal crossing-over, leading to missegregation and aneuploidy, and aberrant exchange between non-allelic homologies are leading causes of congenital disease in humans (Herbert et al., 2015; Hunter, 2015; Kim et al., 2016; Wang et al., 2017).

The regulatory processes that underlie crossover control remain poorly understood. Crossover sites are designated from a larger pool of recombination sites initiated by Spo11-catalyzed DNA double-strand breaks (DSBs)(Lam and Keeney, 2014). DSBs outnumber crossovers by ~2-fold in budding yeast, ~10-fold in mammals and up to 30-fold in some plants. At the cytological level, the differentiation of crossover sites manifests as the selective retention and accumulation of specific recombination factors. One such factor is MutSγ, a heterodimer of Msh4 and Msh5, two homologs of the DNA mismatch-recognition factor MutS (Manhart and Alani, 2016; Snowden et

bioRxiv preprint doi: https://doi.org/10.1101/386458; this version posted August 7, 2018. The copyright holder for this preprint (which was not certified by peer review) is the author/funder, who has granted bioRxiv a license to display the preprint in perpetuity. It is made available under aCC-BY-NC-ND 4.0 International license.

al., 2004). Msh4 and Msh5 are members the ZMM proteins (Zip1, Zip2, Zip3, Zip4, Msh4, Msh5, Mer3, and Spo16), a diverse set of activities that facilitate crossover-specific events of recombination, and couple these events to chromosome synapsis (Fung et al., 2004; Hunter, 2015; Lynn et al., 2007; Shinohara et al., 2008). As seen in a variety of species, initial numbers of MutSγ immunostaining foci greatly outnumber final crossover numbers (De Muyt et al., 2014; de Vries et al., 1999; Edelmann et al., 1999; Higgins et al., 2008; Kneitz et al., 2000; Yokoo et al., 2012; Zhang et al., 2014). As prophase I progresses, MutSγ is lost from most recombination sites but retained at sites that will go on to mature into crossovers. This patterning process is dependent on the Zip3/RNF212/ZHP-3/HEI10 family of RING E3 ligases (Agarwal and Roeder, 2000; Bhalla et al., 2008; Chelysheva et al., 2012; De Muyt et al., 2014; Henderson and Keeney, 2004; Jantsch et al., 2004; Qiao et al., 2014; Rao et al., 2017; Reynolds et al., 2013; Wang et al., 2012; Yokoo et al., 2012; Zhang et al., 2018). Additional evidence implicates the SUMO-modification and ubiquitin-proteasome systems in meiotic crossover control (Ahuja et al., 2017; Rao et al., 2017) and suggests a model in which factors such as MutSγ are selectively stabilized at crossover sites by protecting them from proteolysis. Implicit in this model is the notion that MutSγ may be intrinsically unstable.

Here, we show that regulated proteolysis plays a direct and essential role in meiotic crossing over. Msh4 is identified as an intrinsically unstable protein that is targeted for proteasomal degradation by an N-terminal degron thereby rendering MutSγ inactive for crossing over. Activation of MutSγ occurs by neutralizing the Msh4 degron via Cdc7-catalyzed phosphorylation. Thus, a key meiotic pro-crossover factor is activated by attenuating its proteolysis.

bioRxiv preprint doi: https://doi.org/10.1101/386458; this version posted August 7, 2018. The copyright holder for this preprint (which was not certified by peer review) is the author/funder, who has granted bioRxiv a license to display the preprint in perpetuity. It is made available under aCC-BY-NC-ND 4.0 International license.

RESULTS

The N-terminal Region of Msh4 is Phosphorylated.

The ZMM proteins were surveyed for modifications detectable as electrophoretic-mobility shifts on Western blots. A prominent modified band was detected for Msh4 but not for its partner Msh5 (**Figure 1A**). Treatment of immunoprecipitated Msh4 with λ phosphatase indicated that the modified form is due to phosphorylation (**Figure 1B**). Relative to the majority faster-migrating species, phosphorylated Msh4 appeared with a ≥1 hr delay, its levels peaked at ~22% of total protein, and then disappeared with the same kinetics (**Figure 1C**). To map sites of phosphorylation, Msh4 was immunoprecipitated, fast and slow migrating forms were resolved by electrophoresis, and then analyzed separately by tandem mass spectrometry (MS/MS; **Figure 1D**). Six phosphorylation sites were identified in the slower migrating form of Msh4, all mapping within the first 50 amino acids (S2, S4, S7, S41, T43 and S46; **Figure 1E; Supplemental Figure S1**). In the faster migrating form of Msh4, only phosphorylation at S41 was detected.

Msh4 and Msh5 lack the N-terminal domain I, which is conserved in other MutS proteins (**Figure 1E**)(Yang et al., 2000). Domain I encircles DNA together with MutS domain IV and is intimately involved in DNA binding and mismatch recognition. Absence of domain I from Msh4 and Msh5 is predicted to enlarge the DNA channel such that it can accommodate JM structures and slide on two duplexes (Rakshambikai et al., 2013; Snowden et al., 2004). The functions of the N-terminal regions of Msh4 and Msh5 are otherwise unknown.

Phosphorylation is Essential for the Crossover Function of Msh4.

To determine the functional relevance of Msh4 phosphorylation, we mutated the six identified phosphorylation sites to alanine to prevent phosphorylation, or to aspartic acid to mimic phosphorylation, creating respectively *msh4-6A* and *msh4-6D* alleles (**Figure 2**). Spore viability,

bioRxiv preprint doi: https://doi.org/10.1101/386458; this version posted August 7, 2018. The copyright holder for this preprint (which was not certified by peer review) is the author/funder, who has granted bioRxiv a license to display the preprint in perpetuity. It is made available under aCC-BY-NC-ND 4.0 International license.

indicative of successful meiotic chromosome segregation, was assessed by tetrad dissection and compared to wild-type and *msh4*Δ-null strains (**Figure 2A,B**). Consistent with previous studies (Krishnaprasad et al., 2015; Nishant et al., 2010; Novak et al., 2001; Stahl et al., 2004), *msh4*Δ reduced spore viability to 34.7% and the pattern of spore death was indicative of chromosome missegregation at the first meiotic division, with a preponderance of tetrads containing two or zero viable spores (**Figure 2B**). The pattern of spore death in cells carrying the phosphorylation-defective *msh4-6A* allele was similar to that of the *msh4*Δ null, with an overall viability of 46.7% (P<0.01 compared to wild type, χ^2 test; **Table S1**). By contrast, the phospho-mimetic *msh4-6D* allele supported wild-type levels of spore viability (96.3% and 95.7%, respectively, P=0.42).

In the absence of Msh4, chromosome missegregation and the ensuing spore death are caused by defective crossing over (Krishnaprasad et al., 2015; Nishant et al., 2010; Novak et al., 2001; Stahl et al., 2004). To assess whether phosphorylation is required for the crossover function of Msh4, we measured genetic map distances in a background carrying markers on three different chromosomes (III, VII and VIII; **Figure 2C**). Cumulative map distances showed that *msh4*Δ reduced crossing by 2.1 to 2.7-fold, (**Figure 2D** and **Supplemental Figure S2** and **Table S2**). Similar reductions (2.1 to 2.8-fold) were seen for the *msh4-6A* phosphorylation-defective strain. Thus, phosphorylation is essential for the crossover function of Msh4. For chromosomes VII and VIII, the *msh4-6A* mutation caused slightly larger reductions in crossing over than the *msh4*Δ null. Possibly, phosphorylation-defective Msh4-6A protein is still capable of binding recombination intermediates and thereby impedes processing via alternative crossover pathways mediated by the structure-selective nucleases (De Muyt et al., 2012; Zakharyevich et al., 2012). Consistent with the high spore viability of the phospho-mimetic *msh4-6D* strain, cumulative map distances for this strain were indistinguishable from those of wild type.

bioRxiv preprint doi: https://doi.org/10.1101/386458; this version posted August 7, 2018. The copyright holder for this preprint (which was not certified by peer review) is the author/funder, who has granted bioRxiv a license to display the preprint in perpetuity. It is made available under aCC-BY-NC-ND 4.0 International license.

Previous analysis showed that non-crossover gene conversions are increased in the absence of ZMMs, including Msh5 (and by extension Msh4), due to the continued formation of DSBs when homolog engagement is defective (Thacker et al., 2014). This phenotype was reflected in tetrad data from the *msh4*Δ null strain, which showed a 3.4-fold increase in cumulative gene conversion frequency for the 12 markers in this background (**Figure 2E**; also see **Supplemental Figure S2**). Significantly elevated gene conversion was also seen for *msh4-6A,* which showed a 2.5-fold increase in gene conversions relative to wild type. Unexpectedly, a 1.7-fold increase in gene conversions was observed for the *msh4-6D* strain, the first indication that this phopsho-mimic allele does not possess fully wild-type function.

Crossovers promoted by MutSγ are patterned by interference (Krishnaprasad et al., 2015; Novak et al., 2001; Stahl et al., 2004). One readout of crossover interference is that tetrads with crossovers in a given "test" interval have significantly lower frequencies of crossovers in the neighboring intervals when compared to tetrads that lack crossovers in the test interval (Malkova et al., 2004)(**Figure 2F**). This difference can be expressed as the ratio of map distances for the neighboring interval in the tetrad subsets with or without a crossover in the test interval. Positive crossover interference is indicated by a ratio that is significantly less than one. To address whether Msh4 phosphorylation promotes crossovers with an interference distribution, this analysis was performed for all intervals pairs (**Figure 2F**; also see **Supplemental Figure S3**).

In wild-type tetrads, significant positive crossover interference was detected for all interval pairs except *LEU2–CEN3–MAT* on chromosome III (**Figure 2F**). Consistent with previous analysis (Novak et al., 2001; Stahl et al., 2004), residual crossovers in the *msh4*Δ strain did not show significant positive interference in any interval pair. In fact, significant negative interference – a

bioRxiv preprint doi: https://doi.org/10.1101/386458; this version posted August 7, 2018. The copyright holder for this preprint (which was not certified by peer review) is the author/funder, who has granted bioRxiv a license to display the preprint in perpetuity. It is made available under aCC-BY-NC-ND 4.0 International license.

higher incidence of double crossovers than expected – was detected for one interval pair on chromosome VII (*LYS5-MET13-CYH2*) in *msh4*Δ tetrads. Analogous results were obtained for the *msh4-6A* strain indicating that Msh4 phosphorylation does indeed promote the formation of crossovers that are subject to interference. However, significant positive interference was still detected in one interval pair for *msh4-6A* (*ARG4-THR1-CUP1*). By contrast, crossover interference in the *msh4-6D* strain was similar to wild type, with the exception of one interval pair in which interference was diminished (*LYS5-MET13-CYH2*; **Figure 2F**). These exceptions suggest that the *msh4-6A* strain may not be completely defective for the formation of interfering crossovers, while *msh4-6D* may not be fully competent for this function.

Interference within individual was also analyzed by calculating NPD ratios (**Figure 2G** and **Supplemental Table S4**). In a single interval, a double crossovers event involving all four chromatids results in a nonparental ditype tetrad (NPD). The NPD ratio compares the number of NPDs observed to that expected if there were no crossover interference (Papazian, 1952). A ratio of significantly less than one indicates positive crossover interference. Results of NPD ratio analysis generally confirmed that residual crossovers in the *msh4*Δ and *msh4-6A* strains show little or no interfere, while interference was detected in all but on interval (*CEN3-MAT*) in the *msh4-6D* strain. Notably, positive interference was detected in the *CEN3-MAT* interval in wild-type tetrads again suggesting that *msh4-6D* is slightly defective for crossover interference.

Next, we determined whether crossover assurance is influenced by Msh4 phosphorylation using a strain carrying eight linked intervals that span the length of chromosome III (**Figure 2H** and **Supplemental Table S5**)(Zakharyevich et al., 2010). In wild type, at least one crossover was detected in 98.9% of tetrads indicating highly efficient crossover assurance (**Figure 2I**). Oppositely, crossover assurance was severely defective in the absence of Msh4, with 25.2% of *msh4*Δ tetrads lacking a detectable crossover between chromosome III, consistent with previous

bioRxiv preprint doi: https://doi.org/10.1101/386458; this version posted August 7, 2018. The copyright holder for this preprint (which was not certified by peer review) is the author/funder, who has granted bioRxiv a license to display the preprint in perpetuity. It is made available under aCC-BY-NC-ND 4.0 International license.

analysis (Krishnaprasad et al., 2015). In addition, the fraction of tetrads with a single crossover was increased and multiple crossover classes were diminished in the *msh4*Δ strain relative to wild type (*P*<0.001, *G*-test). If crossover assurance remained operational in *msh4-6A* cells, the residual crossover rate (1.7 crossovers per meiosis) is in principle sufficient to ensure that chromosome III obtains a crossover in every meiosis. Contrary to this scenario, 17.4% of *msh4-6A* tetrads had zero crossovers highlighting the importance of Msh4 phosphorylation for crossover assurance (**Figure 2I**; *P*<0.001 compared to wild type, *G*-test; distributions of crossover classes were not significantly different for *msh4-6A* and *msh4*Δ*, P*=0.11)**.** The phospho-mimetic *msh4-6D* strain was indistinguishable from wild type for crossover assurance with just 2.8% of tetrads lacking a crossover (*P*=0.79). We conclude that phosphorylation of the N-terminus of Msh4 promotes the formation of crossovers that are subject to patterning processes that result in crossover assurance and interference.

The contributions of individual phosphorylation sites to the crossover function of Msh4 were also assessed (**Supplemental Figure S3**). This analysis revealed a major role for phosphorylation at sites S2, S4 and S7, while S41, T43 and S46 made little or no contribution to crossing over. Western analysis indicated that Msh4-6A protein could still be phosphorylated, albeit with a delay and at lower levels than wild-type Msh4 (**Supplementary Figure S5;** low-level phosphorylation was also detected for Msh4-6D; also see **Figure 5A**). This residual phosphorylation was abolished following mutation of all 18 serine and threonine residues present in the first 50 amino acids of Msh4 indicating that phosphorylation leading to the slow migrating form is confined to this to this region. Importantly, the *msh4-18A* strain was no more defective for crossing over than the *msh4-6A* strain, indicating that phosphorylation at other sites in the N-terminus is not functionally redundant with the phosphorylation sites mapped by MS/MS (**Supplementary Figure S3**).

bioRxiv preprint doi: https://doi.org/10.1101/386458; this version posted August 7, 2018. The copyright holder for this preprint (which was not certified by peer review) is the author/funder, who has granted bioRxiv a license to display the preprint in perpetuity. It is made available under aCC-BY-NC-ND 4.0 International license.

Msh4 Phosphorylation Facilitates the Formation and Resolution of DNA Joint Molecules

To understand how the molecular steps of meiotic recombination are influenced by Msh4 phosphorylation, DNA intermediates were monitored in cultures undergoing synchronous meiosis using a series of Southern blot assays at the well-characterized *HIS4::LEU2* recombination hotspot (**Figure 3**)(Hunter and Kleckner, 2001; Oh et al., 2007). At this locus, *Xho*I polymorphisms between the two parental chromosomes produce DNA fragments diagnostic for DSBs, JMs, and crossover products. DSBs, and crossovers were analyzed using one-dimensional (1D) gels (**Figure 3A–C**). Noncrossover products were detected by monitoring conversion of a *Bam*HI/*Ngo*MIV restriction-site polymorphism located directly at the site of DSB formation (**Figure 3A** and **3D**).

Analysis of JM intermediates in budding yeast together with fine-scale analysis of recombination products in a variety of species, indicates that crossover and noncrossover pathways diverge at an early step, following nascent D-loop formation (Allers and Lichten, 2001b; Borner et al., 2004; Drouaud et al., 2013; Guillon et al., 2005; Hunter and Kleckner, 2001; Jeffreys and May, 2004; Marsolier-Kergoat et al., 2018; Martini et al., 2011; Rockmill et al., 2013; Wijnker et al., 2013). A majority of noncrossovers arise from D-loops via synthesis-dependent strand annealing in which the invading 3' end is extended by DNA polymerase, unwound and then annealed to the other DSB end. By contrast, most crossovers form via metastable one-ended strand-exchange intermediates called single-end invasions (SEIs), which form as homologs synapse (Hunter and Kleckner, 2001). Through DNA synthesis and second-end capture, SEIs give rise to double-Holliday junctions (dHJs)(Lao et al., 2008), which must then undergo biased resolution into crossovers (Zakharyevich et al., 2012). Native/native two-dimensional (2D) gels reveal the branched structure of JMs and were used to quantify SEIs, inter-homolog dHJs (IH-dHJs), inter-sister JMs (IS-JMs) and multi-chromatid JMs (mc-JMs) comprising three and four interconnected DNA molecules (**Figure 3E** and **3F**). To monitor the timing and efficiency of

bioRxiv preprint doi: https://doi.org/10.1101/386458; this version posted August 7, 2018. The copyright holder for this preprint (which was not certified by peer review) is the author/funder, who has granted bioRxiv a license to display the preprint in perpetuity. It is made available under aCC-BY-NC-ND 4.0 International license.

meiotic divisions, fixed cells were stained with DAPI and scored as having one, two, or four nuclei.

In wild-type, *msh4*Δ*, msh4-6A* and *msh46D* strains, DSBs appeared and reached peak levels with similar timing (**Figure 3C**). Peak DSB levels were higher and DSBs disappeared with a ~1 hr delay in the *msh4*Δ null mutant relative to wild type, consistent with delayed progression of recombination and continued DSB formation (Borner et al., 2004; Thacker et al., 2014). Delayed progression in *msh4*Δ cells was also reflected by a ~2 hr delay of the meiosis-I division (MI) (**Figure 2C**). Mirroring the crossover reductions detected by tetrad analysis, crossovers at *HIS4::LEU2* were reduced ~2-fold in *msh4*Δ cells. A similar reduction is crossing over was seen for *msh4-6A* cells, but progression defects were less severe than those seen for *msh4*Δ; disappearance of DSBs was delayed by ~30 minutes and MI was delayed by ~1.25 hrs. In *msh4-6D* cells, slight delays (≤20 minutes) in DSB turnover and crossover formation were apparent, but crossovers reached wild-type levels.

The increased rates of gene conversion seen in *msh4*Δ and *msh4-6A* tetrads (**Figure 2E**) were mirrored by elevated levels of non-crossover gene conversions at *HIS4::LEU2* (**Figure 3D**). Again, the effect of *msh4*-6A was weaker than that of the *msh4*Δ null (increases of 1.8-fold versus 3.0-fold, respectively). Although gene conversion was also significantly elevated in *msh4-6D* tetrads, non-crossovers at *HIS4::LEU2* were not significantly increased.

2D gel analysis revealed the importance of Msh4 phosphorylation for JM metabolism (**Figure 3E–H**). In *msh4-6A* cells, formation of all JM species was delayed relative to wild-type by ~30-60 mins (**Figure 3G**), with the longest delays seen for IS-JMs and mc JMs, i.e. JMs involving strand-exchange between sister chromatids. A further delay of ~1.5 hrs was seen for the disappearance of JMs in *msh4-6A* relative to wild type. Peak levels of JM were also lower in

bioRxiv preprint doi: https://doi.org/10.1101/386458; this version posted August 7, 2018. The copyright holder for this preprint (which was not certified by peer review) is the author/funder, who has granted bioRxiv a license to display the preprint in perpetuity. It is made available under aCC-BY-NC-ND 4.0 International license.

msh4-6A cells, averaging 61% of wild-type levels (**Figure 3H**). JM kinetics in *msh4*Δ null mutants were similar to those of *msh4-6A* (**Figure 3G**), but peak JM levels were significantly lower averaging just 40% of wild-type levels (**Figure 3H**). Thus, with respect to DSB persistence, JM levels and prophase delay, the phenotypes of the *msh4-6A* mutant are milder than those of the *msh4*Δ null.

Notably, SEIs reached similar levels in *msh4-6A* and *msh4*Δ cells (% of hybridizing DNA = 1.19% ± 0.05 S.E. and 0.91% ± 0.13 S.E., respectively), but dHJ levels were ~2-fold lower in *msh4*Δ cells (0.83% ± 0.05 S.E. and 0.40% ± 0.02 S.E., respectively). Two non-exclusive possibilities could explain this difference: (i) the SEI-to-dHJ transition is less efficient and/or (ii) the stability of IH-dHJs is lower in the absence of Msh4 than when the Msh4-6A protein is present. However, despite higher IH-dHJ levels in *msh4-6A* cells, final crossover levels are very similar to those of the *msh4*Δ null (**Figures 2D, 2H** and **3C**). Together, these data suggest that phosphorylation of Msh4 is important both for JM formation and the crossover-biased resolution of IH-dHJs into crossovers.

In *msh4-6D* cells, a minor delay in SEI formation was suggested and IH-dHJs peaked at ~24% higher levels relative to wild type (1.58% ± 0.11 versus 1.27% ± 0.11**)**. But overall, JM kinetics and levels in *msh4-6D* cells were similar to those of wild type (**Figure 3G and 3H**).

Msh4 Phosphorylation Facilitates Homolog Synapsis

In most organisms, the strand-exchange step of meiotic recombination promotes the pairing of homologs and their intimate end-to-end connection by synaptonemal complexes (SCs), meiosis-specific structures comprising densely-packed transverse filaments (Zickler and Kleckner, 2015). Crossovers then mature in the context of SCs, which are subsequently disassembled leaving homologs connected only at the sites of exchange. The possibility that the delayed and

bioRxiv preprint doi: https://doi.org/10.1101/386458; this version posted August 7, 2018. The copyright holder for this preprint (which was not certified by peer review) is the author/funder, who has granted bioRxiv a license to display the preprint in perpetuity. It is made available under aCC-BY-NC-ND 4.0 International license.

inefficient JM formation seen in *msh4-6A* cells leads to defective homolog synapsis was addressed by immuno-staining surface-spread nuclei for the synaptonemal complex central-region component Zip1 (**Figure 4A** and **4B**). Synapsis was monitored over time by assigning nuclei to one of three classes based on the pattern of Zip1 staining (Borner et al., 2004): class I nuclei were defined by a dotty pattern; class II nuclei had partial synapsis with both linear and dotty staining; and class III had full synapsis indicated by extensive linear staining. Nuclei containing aggregates of Zip1 called polycomplexes (PCs), a sensitive indicator of synapsis defects (Sym and Roeder, 1995), were also quantified irrespective of their staining class.

In wild-type cells, synapsis was well underway by 4 hrs, peak levels of class III nuclei (35%) with full synapsis were seen at 5 hrs, and Zip1 has disappeared by 8 hrs when cells are completing meiotic divisions (**Figure 4B**). Consistent with previous studies (Borner et al., 2004; Novak et al., 2001), synapsis was severely defective in *msh4*Δ null cells, with only 9% of cells achieving full synapsis and PCs present in a majority of cells. PCs were similarly prominent in *msh4-6A* cells, but synapsis was slightly more efficient, with significantly higher levels of class II and class III nuclei ($P<0.005$, *G*-test). By contrast, synapsis in *msh4-6D* cells was indistinguishable from wild-type cells ($P=0.75$). Thus, Msh4 phosphorylation facilitates the formation and/or stabilization of SCs.

Phosphorylation Promotes Chromosomal Localization of Msh4

To begin to understand how phosphorylation facilitates Msh4 function, the chromosomal localization patterns of Msh4, Msh4-6A and Msh4-6D proteins were compared. Surface spread nuclei were immunostained for both Msh4 and Zip1 (**Figure 4B** and **4C**). Msh4 foci were quantified in nuclei with zygotene (class II) and pachytene (class III) morphologies, i.e. partial and complete lines of Zip1 staining. In wild-type, Msh4 foci averaged 43.9 ± 13.3 S.D. per nucleus while focus numbers in *msh4-6A* nuclei were lower, averaging 33.8 ± 10.4 S.D.

bioRxiv preprint doi: https://doi.org/10.1101/386458; this version posted August 7, 2018. The copyright holder for this preprint (which was not certified by peer review) is the author/funder, who has granted bioRxiv a license to display the preprint in perpetuity. It is made available under aCC-BY-NC-ND 4.0 International license.

(*P*<0.0001, two-tailed Mann Whitney test; **Figure 4C**). By contrast, the Msh4-6D protein formed elevated numbers of foci relative to wild-type Msh4, averaging 47.7 ± 11.3 S.D. per nucleus (*P*=0.028). Phenotypes associated with phosphorylation-defective (*msh4-3A*) and phosphorylation-mimetic (*msh4-3D*) alleles for sites S2, S4 and S7 were analogous to those of *msh4-6A* and *msh4-6D* with respect to formation of Msh4 foci (**Supplementary Figure S4**), further highlighting the importance of these three proximal serine residues.

Msh4 is Stabilized by Phosphorylation

We explored the possibility that aberrant localization of phosphorylation-defective Msh4-6A protein is caused by decreased protein stability. Consistent with this idea, Western analysis showed that Msh4-6A protein levels were lower at all time points during meiosis, averaging a 2.2-fold reduction relative to wild-type Msh4 (**Figure 5A,B** and **Supplemental Figure S5**). In striking contrast, the Msh4-6D protein was hyper-stable, with an average increase of 2.1-fold. However, despite differences in steady-state protein levels, the overall timing of Msh4 appearance and disappearance was quite similar for Msh4, Msh4-6A and Msh4-6D proteins.

Next, we examined whether the lower level of the msh4-6A protein was due to proteasome-mediated degradation. Wild-type and *msh4-6A* cells were treated with the proteasome inhibitor MG132 two hours after transfer to sporulation media and Msh4 protein levels were measured at 4, 5 and 6 hrs by Western blot (**Figure 5C,D**). Consistent with the analysis above, in the absence of MG132, Msh4-6A protein levels were reduced to 21-44% of wild-type levels. Treatment with MG132 restored Msh4-6A levels to between 94% and 125% of Msh4 levels seen in control wild-type cells. MG132 treatment did not have a significant effect on wild-type Msh4 levels at 4 and 5 hrs, but at 6 hrs Msh4 levels were 1.8-fold higher than in untreated cells (**Figure 5C,D**). These data imply that phosphorylation stabilizes Msh4 during meiotic prophase I by protecting it from proteasomal degradation.

bioRxiv preprint doi: https://doi.org/10.1101/386458; this version posted August 7, 2018. The copyright holder for this preprint (which was not certified by peer review) is the author/funder, who has granted bioRxiv a license to display the preprint in perpetuity. It is made available under aCC-BY-NC-ND 4.0 International license.

If the primary function of phosphorylation is to stabilize Msh4, then overexpression of phosphorylation-defective Msh4-6A protein should suppress *msh4-6A* mutant phenotypes. Indeed, overexpression of *msh4-6A* using the strong, copper-inducible *CUP1* promoter restored crossing-over and spore viability to near wild-type levels (**Figure 5E–G**).

The Msh4 N-Terminus Encodes a Portable Degron

Our analysis points to a model in which Msh4 is an intrinsically unstable protein that is stabilized by phosphorylation of N-terminal residues, thereby activating the crossover function of MutSγ. To further test this model, full-length Msh4 and an N-terminally truncated derivative (Msh4-ΔN50) were co-expressed in vegetative (non-meiotic) yeast cells using the *CUP1* promoter (**Figure 5H–J** and **Supplemental Figure S5**). The steady-state level of full-length Msh4 was 3-fold lower than that of Msh4-ΔN50 and treatment with MG132 showed that this difference was due to proteasomal degradation. By contrast, the N-terminus of Msh5 had no effect in its stability (**Supplemental Figure S6**). Thus, the N-terminal region of Msh4 possesses degron activity.

Comparison of protein levels in strains co-expressing wild-type Msh4 and Msh4-ΔN50 versus Msh4-6D and Msh4-ΔN50 revealed that the phospho-mimetic allele significantly attenuated N-terminal degron activity (**Figure 5K–M**)**.** Protein half-lives, estimated from cycloheximide chase experiments, were ~14, 31 and 61 minutes respectively for Msh4, Msh4-6D and Msh4-ΔN50 (**Supplemental Figure S5**).

To address whether the Msh4 N-terminus has autonomous, portable degron activity, residues 1-50 of wild-type Msh4 (“Degron”) or a phospho-mimetic derivative (“Degron(6D)”) were fused to GFP and co-expressed in vegetative cells together with wild-type GFP (**Figure 5N**). The Msh4

bioRxiv preprint doi: https://doi.org/10.1101/386458; this version posted August 7, 2018. The copyright holder for this preprint (which was not certified by peer review) is the author/funder, who has granted bioRxiv a license to display the preprint in perpetuity. It is made available under aCC-BY-NC-ND 4.0 International license.

degron destabilized GFP, reducing its half-life from ~59 to 19 mins (**Figure 5O,P** and **Supplemental Figure S5**). By contrast, stability of the phospho-mimetic Degron(6D)-GFP fusion was similar to that of wild-type GFP (half life of ~49 mins). Together, these data indicate that the N-terminal domain of Msh4 comprises an autonomous degron that is neutralized by phosphorylation.

Evidence That Msh4 Phosphorylation Occurs *In Situ* At Sites of Recombination

The genetic requirements for Msh4 phosphorylation were delineated by performing Western analysis on extracts from mutant strains that are defective for successive steps in meiotic recombination, chromosome pairing and synapsis (**Figure 6A**). The slow migrating band diagnostic of phosphorylated Msh4 was not detected in *spo11-Y135F, mnd1*Δ*, zip1*Δ and *zip3*Δ mutants (**Figure 6B**). The *spo11-Y135F* allele lacks the catalytic tyrosine required for DSB formation and therefore fails to initiate meiotic recombination (Bergerat et al., 1997). Mnd1 is an essential co-factor for DNA strand-exchange and *mnd1*Δ mutant cells are severely defective for DSB repair, homolog pairing and synapsis (Chen et al., 2004; Gerton and DeRisi, 2002; Tsubouchi and Roeder, 2002). *zip1*Δ cells achieve homolog pairing, but formation of crossover-designated JMs is defective and synapsis fails because Zip1 is the major component of the SC central region (Borner et al., 2004; Sym et al., 1993). The SUMO E3 ligase, Zip3, accumulates at future crossover sites and facilitates the loading of other ZMM factors, including MutSγ (Agarwal and Roeder, 2000; Cheng et al., 2006; Henderson and Keeney, 2004; Shinohara et al., 2008). *zip3*Δ mutants are defective for homolog synapsis, JM formation and crossing over (Agarwal and Roeder, 2000; Borner et al., 2004). Thus, Msh4 phosphorylation is DSB dependent and requires synapsis and the formation of crossover designated JMs.

Analysis of two additional mutants, *ndt80*Δ and *mlh3*Δ*,* showed that Msh4 phosphorylation does not require dHJ resolution or crossing over (**Figure 6B**). Ndt80 is a transcription factor required

bioRxiv preprint doi: https://doi.org/10.1101/386458; this version posted August 7, 2018. The copyright holder for this preprint (which was not certified by peer review) is the author/funder, who has granted bioRxiv a license to display the preprint in perpetuity. It is made available under aCC-BY-NC-ND 4.0 International license.

for meiosis to progress beyond pachytene (Chu and Herskowitz, 1998). *ndt80*Δ cells arrest with fully synapsed chromosomes and unresolved JMs (Allers and Lichten, 2001a). In *ndt80*Δ cells, phospho-Msh4 accumulated to very high levels (≥60% of total Msh4) and persisted in arrested cells (**Figure 6B**). The MutLγ complex, comprising MutL homologs Mlh1 and Mlh3, possesses endonuclease activity that is required for the biased resolution of dHJs into crossovers, but not for JM resolution *per se* (Claeys Bouuaert and Keeney, 2017; Manhart et al., 2017; Ranjha et al., 2014; Rogacheva et al., 2014; Zakharyevich et al., 2012). In *mlh3*Δ mutants, chromosomes synapse and normal levels of JMs are formed and resolved, but crossing over is defective (Zakharyevich et al., 2012). Phosphorylation and turnover of Msh4 appeared normal in *mlh3*Δ cells (**Figure 6B**).

Overall, our analysis suggests that Msh4 is phosphorylated *in situ* at sites of recombination, likely when bound to JM intermediates in the context of synapsed chromosomes. Consistent with this inference, chromatin-associated Msh4 was highly enriched for the phosphorylated form relative to soluble Msh4 (**Figure 6C,D**). Specifically, while total Msh4 protein was roughly equally distributed between chromatin-bound and soluble cell fractions, 95% of phospho-Msh4 was found in the chromatin-bound fraction (**Figure 6C,D**).

Msh4 Phosphorylation is Catalyzed by Dbf4-Dependent Kinase, Cdc7

To identify the kinase(s) responsible for Msh4 phosphorylation, the requirements for candidate kinases were systematically analyzed (**Figure 7**; also see **Supplemental Figure S7**). The PI3K-like kinases, Mec1^{ATR} and Tel1^{ATM} are primary sensor kinases of the DNA-damage response and function in meiosis to regulate DSB distribution, inter-homolog template bias and crossing over (Carballo and Cha, 2007; Cooper et al., 2016). Msh4 phosphorylation was reduced more than 2-fold in P_{CLB2}-*MEC1* cells in which the essential *MEC1* gene is expressed under the meiotically-repressed *CLB2* promoter (**Figure 7A** and **B**)(Lee and Amon, 2003). Moreover,

bioRxiv preprint doi: https://doi.org/10.1101/386458; this version posted August 7, 2018. The copyright holder for this preprint (which was not certified by peer review) is the author/funder, who has granted bioRxiv a license to display the preprint in perpetuity. It is made available under aCC-BY-NC-ND 4.0 International license.

residual Msh4 phosphorylation seen in P_{CLB2}-*MEC1* cells was abolished and steady-state protein levels of Msh4 were reduced when Tel1 was also inactivated using a *tel1-kd* kinase-dead allele (Ma and Greider, 2009)(Msh4 phosphorylation was unaffected in the *tel1-kd* single mutant).

None of the identified Msh4 phosphorylation sites conform to the S/T-Q Mec1/Tel1 target-site consensus (**Figure 1E**), making it unlikely to be a direct target. Thus, we explored whether signaling pathways downstream of Mec1/Tel1 are important for Msh4 phosphorylation. An important meiotic target of Mec1/Tel1 is Hop1, a checkpoint adaptor for the meiotic DNA damage response that recruits and activates the serine/threonine effector kinase, Mek1 (Carballo et al., 2008; Niu et al., 2005). Mek1 promotes inter-homolog bias, synapsis and crossing over, and regulates meiotic progression (Callender et al., 2016; Chen et al., 2015; Hollingsworth, 2010; Niu et al., 2007; Prugar et al., 2017; Subramanian et al., 2016; Wu et al., 2010). Although Mek1 consensus-target sites (RXXT) are absent from the Msh4 N-terminus, a *mek1*Δ null mutation abolished Msh4 phosphorylation and reduced steady-state protein levels (**Figure 7C**). Diminished Msh4 phosphorylation in *mek1*Δ cells could be an indirect effect of the defective inter-homolog interactions caused by this mutation. Therefore, we employed a chemical genetic approach to inhibit Mek1 kinase activity after inter-homolog interactions and synapsis have been established (**Figure 7D**). Inhibition of the analog-sensitive *mek1-as* allele (Wan et al., 2004) at 5 hrs after transfer to sporulation media resulted in the rapid disappearance of phosphorylated Msh4 and a reduction in Msh4 protein levels (**Figure 7D** and **E**). To test whether Msh4 is a direct substrate of Mek1, recombinant MutSγ was incubated with immuno-purified Mek1-as (**Figure 7F**). Phosphorylation catalyzed specifically by Mek1-as was detected using the ATPγS analog, N^6-furfuryl-ATPγS, and the semi-synthetic epitope system

bioRxiv preprint doi: https://doi.org/10.1101/386458; this version posted August 7, 2018. The copyright holder for this preprint (which was not certified by peer review) is the author/funder, who has granted bioRxiv a license to display the preprint in perpetuity. It is made available under aCC-BY-NC-ND 4.0 International license.

(Allen et al., 2007; Lo and Hollingsworth, 2011). Under these conditions, only auto-phosphorylation of Mek1-as was detected indicating that Msh4 is not a direct target of Mek1.

Dbf4-dependent kinase (DDK) comprises the kinase Cdc7 and regulatory subunit Dbf4 (Matsumoto and Masai, 2013). DDK functions throughout meiosis and promotes ZMM-mediated crossing over through phosphorylation of Zip1 (Chen et al., 2015). Analogous to *mek1-as,* inhibition of the analog-sensitive *cdc7-as* allele (Wan et al., 2006) at 5 hrs (after Cdc7 has activated DSB and SC formation) caused rapid disappearance of phosphorylated Msh4 accompanied by a reduction in total protein level (**Figure 7G** and **H**).

In vitro phosphorylation reactions showed that DDK was able to directly phosphorylate the Msh4 N-terminus (**Figure 7I**). To specifically detect phosphorylation catalyzed by Cdc7, immuno-purified Cdc7-as/Dbf4 complex was incubated with 6-benzyl-ATPγS and phosphorylation was detected via the semi-synthetic epitope system (Allen et al., 2007; Chen et al., 2015; Lo and Hollingsworth, 2011). In the absence of recombinant MutSγ, only auto-phosphorylation of Cdc7-as and Dbf4 was detected. When wild-type MutSγ ("WT" in **Figure 7I**) was added, an additional phosphorylation product was detected corresponding to the molecular weight of Msh4. The identity of this product was confirmed in two ways. First, MutSγ derivatives containing Msh4-3A ("3A" mutant for S2, S4 and S7) or Msh4-6A ("6A") proteins were used as substrates. Phosphorylation of Msh4-3A was reduced by 68% relative to wild type, while Msh4-6A was not modified by DDK (**Figure 7I**). Second, when Msh4, Msh4-3A and Msh4-6A proteins were purified from DDK kinase assay mixtures, identical phosphorylation patterns were detected. In addition, all phosphorylation products were sensitive to inhibition of Cdc7-as by PP1, confirming the specificity of this reaction. Phosphorylation of Msh5 was not detected indicating that DDK regulates MutSγ by specifically targeting Msh4.

bioRxiv preprint doi: https://doi.org/10.1101/386458; this version posted August 7, 2018. The copyright holder for this preprint (which was not certified by peer review) is the author/funder, who has granted bioRxiv a license to display the preprint in perpetuity. It is made available under aCC-BY-NC-ND 4.0 International license.

DISCUSSION

Regulated Proteolysis Is a Key Aspect of Meiotic Crossing Over

The molecular mechanisms that underpin the differentiation of meiotic crossover and non-crossover pathways have remained elusive. Specifically, how events leading to dHJ formation are facilitated at some recombination sites but not at others, and how dHJs maintain their crossover fate and undergo crossover-biased resolution. Here, regulated proteolysis is revealed as a key determinant of crossing over. This discovery substantiates previous studies implicating the ubiquitin-proteasome system (UPS) in crossover/non-crossover differentiation (Ahuja et al., 2017; Qiao et al., 2014; Rao et al., 2017; Reynolds et al., 2013). Notably, when the UPS is inactivated in mouse spermatocytes, meiotic recombination stalls and ZMM factors (including MutSγ) persist at sites that would normally mature into non-crossovers, suggesting that ZMMs may be targeted for proteolysis at these sites (Rao et al., 2017). At least one ZMM factor, Msh4, can now be designated as a direct target of proteasomal degradation. The atypical mode of Msh4 regulation reveals unanticipated facets of crossover differentiation: intrinsic instability of an essential factor dictates that non-crossover will be the default outcome, and kinase-dependent stabilization activates crossing over.

The Crossover Activity of MutSγ Is Activated by Stabilizing Msh4

Distinct activities of the ZMMs influence different aspects of crossover maturation and couple these events to homolog synapsis. The DNA helicase, Mer3, functions both to regulate the extension of nascent D-loops by DNA synthesis and stabilize JMs (Borner et al., 2004; Duroc et al., 2017; Mazina et al., 2004; Nakagawa and Kolodner, 2002); the XPF-ERCC1 related complex, Zip2-Spo16, specifically binds JMs (De Muyt et al., 2018; Guiraldelli et al., 2018;

bioRxiv preprint doi: https://doi.org/10.1101/386458; this version posted August 7, 2018. The copyright holder for this preprint (which was not certified by peer review) is the author/funder, who has granted bioRxiv a license to display the preprint in perpetuity. It is made available under aCC-BY-NC-ND 4.0 International license.

Macaisne et al., 2011); Zip1 acts both locally to promote ZMM function and globally as the major component of SCs (Chen et al., 2015; Sym et al., 1993; Voelkel-Meiman et al., 2015); Zip3 is a SUMO E3 ligase that helps localize other ZMMs to nascent crossover sites and facilitates synapsis (Agarwal and Roeder, 2000; Cheng et al., 2006; Macqueen and Roeder, 2009; Shinohara et al., 2008); and Zip4 is a large TPR repeat protein thought to bridge interactions between Zip2-Spo16, Zip3, MutSγ and the chromosome axis protein Red1 (De Muyt et al., 2018). Several activities are ascribed to MutSγ: (i) specific binding to JM structures (D-loops and Holliday junctions)(Snowden et al., 2004); (ii) stabilization of nascent JMs following ATP-dependent conversion of JM-bound MutSγ into a sliding clamp that diffuse away from the junction point while embracing two DNA duplexes (Snowden et al., 2004); (iii) protection of dHJs from the anti-crossover "dissolution" activity of the STR decatenase complex, Sgs1–Top3–Rmi1 (equivalent to the human BTR complex, BLM–TOPIIIα–RMI1/2)(Jessop et al., 2006; Kaur et al., 2015; Oh et al., 2007; Tang et al., 2015)(Tang and Hunter, unpublished); (iv) direct or indirect recruitment and activation of crossover-biased JM resolving factors such as the MutLγ endonuclease (Manhart et al., 2017; Nishant et al., 2008; Ranjha et al., 2014; Zakharyevich et al., 2012); (v) formation and/or stabilization of homolog synapsis (Borner et al., 2004; Novak et al., 2001).

Phosphorylation-defective Msh4-6A protein can still localize to chromosomes and retains significant function for synapsis and JM formation. However, the essential crossover function(s) of MutSγ is inactive unless Msh4 is stabilized by phosphorylated. We suggest that these essential functions are to protect dHJs from STR/BTR-mediated dissolution and facilitate their biased resolution. This proposal is also consonant with our inference that DDK targets MutSγ complexes that have bound JMs in the context of synapsed or synapsing chromosomes. Notably, STR/BTR complexes also accumulate at crossover sites (Jagut et al., 2016; Rockmill

bioRxiv preprint doi: https://doi.org/10.1101/386458; this version posted August 7, 2018. The copyright holder for this preprint (which was not certified by peer review) is the author/funder, who has granted bioRxiv a license to display the preprint in perpetuity. It is made available under aCC-BY-NC-ND 4.0 International license.

et al., 2003; Woglar and Villeneuve, 2018); and the symmetric arrangement of dual foci of MutSγ and BTR observed in *C. elegans* suggests a specific model in which MutSγ sliding clamps accumulate between the two junctions of a dHJ to impede dissolution (Woglar and Villeneuve, 2018). We propose that sliding clamps of MutSγ must accumulate above a minimum number in order to facilitate crossing over, be it through dHJ stabilization, recruitment or activation of resolving enzymes, or maintaining dHJs in a geometry that is conducive to crossover-biased resolution. Under this model, the requisite threshold of dHJ-bound MutSγ clamps requires the stabilization of Msh4 by phosphorylation. We note that estimated half-life of stabilized Msh4 (30-60 mins) is similar to the estimated lifespan of dHJs (Allers and Lichten, 2001a; Hunter and Kleckner, 2001) suggesting a causal relationship.

If MutSγ were the primary limiting factor for crossing over, then the hyper-stable phospho-mimetic Msh4-6D protein would be expected to increase crossing over. Although *msh4-6D* strains showed modest increases in Msh4 foci and IH-dHJs, elevated gene conversion and mildly perturbed interference, crossing over was not increased. Thus, some other factor(s) limits crossover numbers. The most likely interpretation is that crossovers are limited by interference and stabilization of Msh4 occurs at designated crossover sites, downstream of the initial crossover/non-crossover decision. However, the proteolysis mechanism revealed here for Msh4 could be a general mechanism to regulate the availability of essential crossover factors and thereby limit crossovers.

We further suggest that the intrinsic instability of Msh4 may be enhanced by proximity to proteasomes, which are recruited in high numbers along chromosome axes as they synapse (Ahuja et al., 2017; Rao et al., 2017). This SC-associated population of proteasomes could

bioRxiv preprint doi: https://doi.org/10.1101/386458; this version posted August 7, 2018. The copyright holder for this preprint (which was not certified by peer review) is the author/funder, who has granted bioRxiv a license to display the preprint in perpetuity. It is made available under aCC-BY-NC-ND 4.0 International license.

accelerate the loss of MutSγ from synapsed sites where Msh4 is not stabilized by phosphorylation and thereby drive recombination towards a non-crossover outcome.

Whether MutSγ is similarly regulated in other organisms remains unclear. An N-terminal region appears to be common to all Msh4 proteins, but sequence conservation is low. However, these regions are typically S/T rich, contain candidate DDK sites and are predicted to undergo disorder-enhanced phosphorylation (**Supplemental Figure S1** and data not shown). The intrinsic stability of Msh4 would presumably have to coevolve with the duration of meiotic prophase in different species, which can vary by at least an order of magnitude.

DDK Is A Key Effector of Meiotic Prophase

In addition to stabilizing Msh4 to activate MutSγ for crossing over, DDK facilitates meiotic S-phase (Valentin et al., 2006; Wan et al., 2006); triggers DSBs and couples their formation to the passage of replication forks (Matos et al., 2008; Murakami and Keeney, 2014; Sasanuma et al., 2008; Wan et al., 2008); promotes synapsis and crossing over via phosphorylation of Zip1 (Chen et al., 2015); enables progression beyond pachytene by removing the Sum1 repressive complex from the *NDT80* promoter (Lo et al., 2012; Lo et al., 2008); drives the destruction of SCs (Argunhan et al., 2017); is required to recruit monopolin to kinetochores enabling mono-orientation of homologs on the meiosis-I spindle (Lo et al., 2008; Matos et al., 2008); and facilitates the cleavage of cohesin to allow homolog disjunction at the meiosis-I division (Katis et al., 2010). Thus, DDK is a primary effector kinase for all the major events of meiotic prophase.

Targeting of both Zip1 and Msh4 implies that DDK is a general activator of ZMM-mediated crossing over. However, the timing, requirements and modes of regulation are distinct. By contrast to Msh4, Zip1 phosphorylation is an early event that depends on DSB formation but not

bioRxiv preprint doi: https://doi.org/10.1101/386458; this version posted August 7, 2018. The copyright holder for this preprint (which was not certified by peer review) is the author/funder, who has granted bioRxiv a license to display the preprint in perpetuity. It is made available under aCC-BY-NC-ND 4.0 International license.

later steps of recombination and doesn't act by stabilizing the protein (Chen et al., 2015). Moreover, Zip1 phosphorylation was inferred to function upstream of the other ZMMs. Consistently, Msh4 phosphorylation requires both the presence of Zip1 and its phosphorylation (**Figure 6** and data not shown). It's unclear how DDK achieves successive, dependent phosphorylation of Zip1 and Msh4. An intriguing possibility is that DDK is sequestered by Zip1 until synapsis ensues, a model suggested by recent analysis of substrate ordering in mitotically cycling cells (Seoane and Morgan, 2017). Alternatively, the N-terminal region of Msh4 could be masked until MutSγ converts to a sliding clamp on DNA; or crossover-designated recombination complexes could create composite docking sites for DDK. Apparent ordering could involve rapid reversal of DDK-catalyzed phosphorylation until Msh4 becomes protected at designated crossover sites. With this model in mind, Woglar and Villeneuve recently demonstrated that crossover-designated recombination complexes become enveloped in "bubbles" of SC central region proteins that could protect components from both phosphatases and proteasomes (Woglar and Villeneuve, 2018).

Contingent Kinase Cascades Order The Events of Meiotic Prophase

While DKK appears to be the ultimate effector for many prophase events, other kinases dictate its activity in space and time. CDK primes DDK phosphorylation of Mer2 to trigger DSB formation (Henderson et al., 2006; Sasanuma et al., 2008; Wan et al., 2008). DSB-dependent activation of $Mec1^{ATR}/Tel1^{ATM}$ locally activates Mek1 (Carballo et al., 2008), which promotes inter-homolog recombination via its direct targets (Callender et al., 2016; Niu et al., 2009), and indirectly activates synapsis and the ZMM pathway by licensing DDK to phosphorylate Zip1 and subsequently Msh4 (Chen et al., 2015)(this study). CDK, DDK and the meiosis-specific kinase Ime2 collectively target the Sum1 transcriptional repressor allowing expression of the transcription factor Ndt80 and exit from pachytene. The polo-like kinase Cdc5, whose expression is Ndt80 dependent, then collaborates with CDK and DDK to disassemble SCs

bioRxiv preprint doi: https://doi.org/10.1101/386458; this version posted August 7, 2018. The copyright holder for this preprint (which was not certified by peer review) is the author/funder, who has granted bioRxiv a license to display the preprint in perpetuity. It is made available under aCC-BY-NC-ND 4.0 International license.

(Argunhan et al., 2017). Cdc5 also collaborates with DDK to localize the monopolin complex to MI kinetochores Lo, 2008 #2913}(Matos et al., 2008). Finally, casein kinase δ/ε works with DDK to activate the cleavage of cohesin by separase and trigger the meiosis-I division (Katis et al., 2010). Understanding the spatial-temporal regulation of DDK with respect to the activation of ZMM dependent crossing over, and its relationship to crossover control are important goals for the future.

EXPERIMENTAL PROCEDURES

Extended methods are described in the Supplemental Information.

SUPPLEMENTAL INFORMATION

Supplemental Information includes extended methods, 7 figures and 7 tables.

ACKNOWLEDGEMENTS

We thank Akira Shinohara, Angelika Amon and Kunihiro Ohta for plasmids and antibodies, and the Hunter Lab for support and discussions. This work was supported by NIH NIGMS grant GM074223 (to N.H.) S.T. was supported by an NIH NIEHS-funded training program in Environmental Health Sciences (T32 ES007058). N.H. is an Investigator of the Howard Hughes Medical Institute.

AUTHOR CONTRIBUTIONS

W.H. and N.H. conceived the study and designed the experiments. W.H., H.B.D.P.R., S.T., N.B., D.K., Y.M., M.C., C.H., J.W-B., H.S.M., C.B., G.F.V., L.C., X.C., and N.H. performed the experiments and analyzed the data. W.H. and N.H. wrote the manuscript with inputs and edits from all authors.

bioRxiv preprint doi: https://doi.org/10.1101/386458; this version posted August 7, 2018. The copyright holder for this preprint (which was not certified by peer review) is the author/funder, who has granted bioRxiv a license to display the preprint in perpetuity. It is made available under aCC-BY-NC-ND 4.0 International license.

DECLARATION OF INTERESTS

The authors declare no competing interests.

REFERENCES

Agarwal, S., and Roeder, G.S. (2000). Zip3 provides a link between recombination enzymes and synaptonemal complex proteins. Cell *102*, 245-255.

Ahuja, J.S., Sandhu, R., Mainpal, R., Lawson, C., Henley, H., Hunt, P.A., Yanowitz, J.L., and Borner, G.V. (2017). Control of meiotic pairing and recombination by chromosomally tethered 26S proteasome. Science *355*, 408-411.

Allen, J.J., Li, M., Brinkworth, C.S., Paulson, J.L., Wang, D., Hubner, A., Chou, W.H., Davis, R.J., Burlingame, A.L., Messing, R.O.*, et al.* (2007). A semisynthetic epitope for kinase substrates. Nature methods *4*, 511-516.

Allers, T., and Lichten, M. (2001a). Differential timing and control of noncrossover and crossover recombination during meiosis. Cell *106*, 47-57.

Allers, T., and Lichten, M. (2001b). Intermediates of yeast meiotic recombination contain heteroduplex DNA. Molecular cell *8*, 225-231.

Argunhan, B., Leung, W.K., Afshar, N., Terentyev, Y., Subramanian, V.V., Murayama, Y., Hochwagen, A., Iwasaki, H., Tsubouchi, T., and Tsubouchi, H. (2017). Fundamental cell cycle kinases collaborate to ensure timely destruction of the synaptonemal complex during meiosis. The EMBO journal *36*, 2488-2509.

Bergerat, A., de Massy, B., Gadelle, D., Varoutas, P.C., Nicolas, A., and Forterre, P. (1997). An atypical topoisomerase II from Archaea with implications for meiotic recombination. Nature *386*, 414-417.

Bhalla, N., Wynne, D.J., Jantsch, V., and Dernburg, A.F. (2008). ZHP-3 acts at crossovers to couple meiotic recombination with synaptonemal complex disassembly and bivalent formation in C. elegans. PLoS genetics *4*, e1000235.

bioRxiv preprint doi: https://doi.org/10.1101/386458; this version posted August 7, 2018. The copyright holder for this preprint (which was not certified by peer review) is the author/funder, who has granted bioRxiv a license to display the preprint in perpetuity. It is made available under aCC-BY-NC-ND 4.0 International license.

Borner, G.V., Kleckner, N., and Hunter, N. (2004). Crossover/noncrossover differentiation, synaptonemal complex formation, and regulatory surveillance at the leptotene/zygotene transition of meiosis. Cell *117*, 29-45.

Callender, T.L., Laureau, R., Wan, L., Chen, X., Sandhu, R., Laljee, S., Zhou, S., Suhandynata, R.T., Prugar, E., Gaines, W.A.*, et al.* (2016). Mek1 Down Regulates Rad51 Activity during Yeast Meiosis by Phosphorylation of Hed1. PLoS genetics *12*, e1006226.

Carballo, J.A., and Cha, R.S. (2007). Meiotic roles of Mec1, a budding yeast homolog of mammalian ATR/ATM. Chromosome Res *15*, 539-550.

Carballo, J.A., Johnson, A.L., Sedgwick, S.G., and Cha, R.S. (2008). Phosphorylation of the axial element protein Hop1 by Mec1/Tel1 ensures meiotic interhomolog recombination. Cell *132*, 758-770.

Chelysheva, L., Vezon, D., Chambon, A., Gendrot, G., Pereira, L., Lemhemdi, A., Vrielynck, N., Le Guin, S., Novatchkova, M., and Grelon, M. (2012). The Arabidopsis HEI10 is a new ZMM protein related to Zip3. PLoS genetics *8*, e1002799.

Chen, X., Suhandynata, R.T., Sandhu, R., Rockmill, B., Mohibullah, N., Niu, H., Liang, J., Lo, H.C., Miller, D.E., Zhou, H.*, et al.* (2015). Phosphorylation of the Synaptonemal Complex Protein Zip1 Regulates the Crossover/Noncrossover Decision during Yeast Meiosis. PLoS biology *13*, e1002329.

Chen, Y.K., Leng, C.H., Olivares, H., Lee, M.H., Chang, Y.C., Kung, W.M., Ti, S.C., Lo, Y.H., Wang, A.H., Chang, C.S.*, et al.* (2004). Heterodimeric complexes of Hop2 and Mnd1 function with Dmc1 to promote meiotic homolog juxtaposition and strand assimilation. Proceedings of the National Academy of Sciences of the United States of America *101*, 10572-10577.

Cheng, C.H., Lo, Y.H., Liang, S.S., Ti, S.C., Lin, F.M., Yeh, C.H., Huang, H.Y., and Wang, T.F. (2006). SUMO modifications control assembly of synaptonemal complex and polycomplex in meiosis of Saccharomyces cerevisiae. Genes & development *20*, 2067-2081.

bioRxiv preprint doi: https://doi.org/10.1101/386458; this version posted August 7, 2018. The copyright holder for this preprint (which was not certified by peer review) is the author/funder, who has granted bioRxiv a license to display the preprint in perpetuity. It is made available under aCC-BY-NC-ND 4.0 International license.

Chu, S., and Herskowitz, I. (1998). Gametogenesis in yeast is regulated by a transcriptional cascade dependent on Ndt80. Molecular cell *1*, 685-696.

Claeys Bouuaert, C., and Keeney, S. (2017). Distinct DNA-binding surfaces in the ATPase and linker domains of MutLgamma determine its substrate specificities and exert separable functions in meiotic recombination and mismatch repair. PLoS genetics *13*, e1006722.

Cooper, T.J., Garcia, V., and Neale, M.J. (2016). Meiotic DSB patterning: A multifaceted process. Cell cycle *15*, 13-21.

De Muyt, A., Jessop, L., Kolar, E., Sourirajan, A., Chen, J., Dayani, Y., and Lichten, M. (2012). BLM helicase ortholog Sgs1 is a central regulator of meiotic recombination intermediate metabolism. Molecular cell *46*, 43-53.

De Muyt, A., Pyatnitskaya, A., Andreani, J., Ranjha, L., Ramus, C., Laureau, R., Fernandez-Vega, A., Holoch, D., Girard, E., Govin, J.*, et al.* (2018). A meiotic XPF-ERCC1-like complex recognizes joint molecule recombination intermediates to promote crossover formation. Genes & development *32*, 283-296.

De Muyt, A., Zhang, L., Piolot, T., Kleckner, N., Espagne, E., and Zickler, D. (2014). E3 ligase Hei10: a multifaceted structure-based signaling molecule with roles within and beyond meiosis. Genes & development *28*, 1111-1123.

de Vries, S.S., Baart, E.B., Dekker, M., Siezen, A., de Rooij, D.G., de Boer, P., and te Riele, H. (1999). Mouse MutS-like protein Msh5 is required for proper chromosome synapsis in male and female meiosis. Genes & development *13*, 523-531.

Drouaud, J., Khademian, H., Giraut, L., Zanni, V., Bellalou, S., Henderson, I.R., Falque, M., and Mezard, C. (2013). Contrasted patterns of crossover and non-crossover at Arabidopsis thaliana meiotic recombination hotspots. PLoS genetics *9*, e1003922.

Duroc, Y., Kumar, R., Ranjha, L., Adam, C., Guerois, R., Md Muntaz, K., Marsolier-Kergoat, M.C., Dingli, F., Laureau, R., Loew, D.*, et al.* (2017). Concerted action of the MutLbeta heterodimer and Mer3 helicase regulates the global extent of meiotic gene conversion. eLife *6*.

bioRxiv preprint doi: https://doi.org/10.1101/386458; this version posted August 7, 2018. The copyright holder for this preprint (which was not certified by peer review) is the author/funder, who has granted bioRxiv a license to display the preprint in perpetuity. It is made available under aCC-BY-NC-ND 4.0 International license.

Edelmann, W., Cohen, P.E., Kneitz, B., Winand, N., Lia, M., Heyer, J., Kolodner, R., Pollard, J.W., and Kucherlapati, R. (1999). Mammalian MutS homologue 5 is required for chromosome pairing in meiosis. Nature genetics *21*, 123-127.

Fung, J.C., Rockmill, B., Odell, M., and Roeder, G.S. (2004). Imposition of crossover interference through the nonrandom distribution of synapsis initiation complexes. Cell *116*, 795-802.

Gerton, J.L., and DeRisi, J.L. (2002). Mnd1p: an evolutionarily conserved protein required for meiotic recombination. Proceedings of the National Academy of Sciences of the United States of America *99*, 6895-6900.

Guillon, H., Baudat, F., Grey, C., Liskay, R.M., and de Massy, B. (2005). Crossover and noncrossover pathways in mouse meiosis. Molecular cell *20*, 563-573.

Guiraldelli, M.F., Felberg, A., Almeida, L.P., Parikh, A., de Castro, R.O., and Pezza, R.J. (2018). SHOC1 is a ERCC4-(HhH)2-like protein, integral to the formation of crossover recombination intermediates during mammalian meiosis. PLoS genetics *14*, e1007381.

Henderson, K.A., Kee, K., Maleki, S., Santini, P.A., and Keeney, S. (2006). Cyclin-dependent kinase directly regulates initiation of meiotic recombination. Cell *125*, 1321-1332.

Henderson, K.A., and Keeney, S. (2004). Tying synaptonemal complex initiation to the formation and programmed repair of DNA double-strand breaks. Proceedings of the National Academy of Sciences of the United States of America *101*, 4519-4524.

Herbert, M., Kalleas, D., Cooney, D., Lamb, M., and Lister, L. (2015). Meiosis and maternal aging: insights from aneuploid oocytes and trisomy births. Cold Spring Harbor perspectives in biology *7*, a017970.

Higgins, J.D., Vignard, J., Mercier, R., Pugh, A.G., Franklin, F.C., and Jones, G.H. (2008). AtMSH5 partners AtMSH4 in the class I meiotic crossover pathway in Arabidopsis thaliana, but is not required for synapsis. Plant J *55*, 28-39.

bioRxiv preprint doi: https://doi.org/10.1101/386458; this version posted August 7, 2018. The copyright holder for this preprint (which was not certified by peer review) is the author/funder, who has granted bioRxiv a license to display the preprint in perpetuity. It is made available under aCC-BY-NC-ND 4.0 International license.

Hillers, K.J., and Villeneuve, A.M. (2003). Chromosome-wide control of meiotic crossing over in C. elegans. Current biology : CB *13*, 1641-1647.

Hollingsworth, N.M. (2010). Phosphorylation and the creation of interhomolog bias during meiosis in yeast. Cell cycle *9*, 436-437.

Hunter, N. (2015). Meiotic Recombination: The Essence of Heredity. Cold Spring Harbor perspectives in biology *7*.

Hunter, N., and Kleckner, N. (2001). The single-end invasion: an asymmetric intermediate at the double-strand break to double-holliday junction transition of meiotic recombination. Cell *106*, 59-70.

Jagut, M., Hamminger, P., Woglar, A., Millonigg, S., Paulin, L., Mikl, M., Dello Stritto, M.R., Tang, L., Habacher, C., Tam, A.*, et al.* (2016). Separable Roles for a Caenorhabditis elegans RMI1 Homolog in Promoting and Antagonizing Meiotic Crossovers Ensure Faithful Chromosome Inheritance. PLoS biology *14*, e1002412.

Jantsch, V., Pasierbek, P., Mueller, M.M., Schweizer, D., Jantsch, M., and Loidl, J. (2004). Targeted gene knockout reveals a role in meiotic recombination for ZHP-3, a Zip3-related protein in Caenorhabditis elegans. Molecular and cellular biology *24*, 7998-8006.

Jeffreys, A.J., and May, C.A. (2004). Intense and highly localized gene conversion activity in human meiotic crossover hot spots. Nature genetics *36*, 151-156.

Jessop, L., Rockmill, B., Roeder, G.S., and Lichten, M. (2006). Meiotic chromosome synapsis-promoting proteins antagonize the anti-crossover activity of sgs1. PLoS genetics *2*, e155.

Jones, G.H. (1984). The control of chiasma distribution. Symposia of the Society for Experimental Biology *38*, 293-320.

Katis, V.L., Lipp, J.J., Imre, R., Bogdanova, A., Okaz, E., Habermann, B., Mechtler, K., Nasmyth, K., and Zachariae, W. (2010). Rec8 phosphorylation by casein kinase 1 and Cdc7-Dbf4 kinase regulates cohesin cleavage by separase during meiosis. Developmental cell *18*, 397-409.

bioRxiv preprint doi: https://doi.org/10.1101/386458; this version posted August 7, 2018. The copyright holder for this preprint (which was not certified by peer review) is the author/funder, who has granted bioRxiv a license to display the preprint in perpetuity. It is made available under aCC-BY-NC-ND 4.0 International license.

Kaur, H., De Muyt, A., and Lichten, M. (2015). Top3-Rmi1 DNA single-strand decatenase is integral to the formation and resolution of meiotic recombination intermediates. Molecular cell *57*, 583-594.

Kim, S., Peterson, S.E., Jasin, M., and Keeney, S. (2016). Mechanisms of germ line genome instability. Semin Cell Dev Biol *54*, 177-187.

Kneitz, B., Cohen, P.E., Avdievich, E., Zhu, L., Kane, M.F., Hou, H., Jr., Kolodner, R.D., Kucherlapati, R., Pollard, J.W., and Edelmann, W. (2000). MutS homolog 4 localization to meiotic chromosomes is required for chromosome pairing during meiosis in male and female mice. Genes & development *14*, 1085-1097.

Krishnaprasad, G.N., Anand, M.T., Lin, G., Tekkedil, M.M., Steinmetz, L.M., and Nishant, K.T. (2015). Variation in crossover frequencies perturb crossover assurance without affecting meiotic chromosome segregation in Saccharomyces cerevisiae. Genetics *199*, 399-412.

Lam, I., and Keeney, S. (2014). Mechanism and regulation of meiotic recombination initiation. Cold Spring Harbor perspectives in biology *7*, a016634.

Lao, J.P., Cloud, V., Huang, C.C., Grubb, J., Thacker, D., Lee, C.Y., Dresser, M.E., Hunter, N., and Bishop, D.K. (2013). Meiotic crossover control by concerted action of rad51-dmc1 in homolog template bias and robust homeostatic regulation. PLoS genetics *9*, e1003978.

Lao, J.P., Oh, S.D., Shinohara, M., Shinohara, A., and Hunter, N. (2008). Rad52 promotes postinvasion steps of meiotic double-strand-break repair. Molecular cell *29*, 517-524.

Lee, B.H., and Amon, A. (2003). Role of Polo-like kinase CDC5 in programming meiosis I chromosome segregation. Science *300*, 482-486.

Lo, H.C., and Hollingsworth, N.M. (2011). Using the semi-synthetic epitope system to identify direct substrates of the meiosis-specific budding yeast kinase, Mek1. Methods in molecular biology *745*, 135-149.

bioRxiv preprint doi: https://doi.org/10.1101/386458; this version posted August 7, 2018. The copyright holder for this preprint (which was not certified by peer review) is the author/funder, who has granted bioRxiv a license to display the preprint in perpetuity. It is made available under aCC-BY-NC-ND 4.0 International license.

Lo, H.C., Kunz, R.C., Chen, X., Marullo, A., Gygi, S.P., and Hollingsworth, N.M. (2012). Cdc7-Dbf4 is a gene-specific regulator of meiotic transcription in yeast. Molecular and cellular biology *32*, 541-557.

Lo, H.C., Wan, L., Rosebrock, A., Futcher, B., and Hollingsworth, N.M. (2008). Cdc7-Dbf4 regulates NDT80 transcription as well as reductional segregation during budding yeast meiosis. Molecular biology of the cell *19*, 4956-4967.

Lynn, A., Soucek, R., and Borner, G.V. (2007). ZMM proteins during meiosis: Crossover artists at work. Chromosome Res *15*, 591-605.

Ma, Y., and Greider, C.W. (2009). Kinase-independent functions of TEL1 in telomere maintenance. Molecular and cellular biology *29*, 5193-5202.

Macaisne, N., Vignard, J., and Mercier, R. (2011). SHOC1 and PTD form an XPF-ERCC1-like complex that is required for formation of class I crossovers. Journal of cell science *124*, 2687-2691.

Macqueen, A.J., and Roeder, G.S. (2009). Fpr3 and Zip3 ensure that initiation of meiotic recombination precedes chromosome synapsis in budding yeast. Current biology : CB *19*, 1519-1526.

Malkova, A., Swanson, J., German, M., McCusker, J.H., Housworth, E.A., Stahl, F.W., and Haber, J.E. (2004). Gene conversion and crossing over along the 405-kb left arm of Saccharomyces cerevisiae chromosome VII. Genetics *168*, 49-63.

Manhart, C.M., and Alani, E. (2016). Roles for mismatch repair family proteins in promoting meiotic crossing over. DNA repair *38*, 84-93.

Manhart, C.M., Ni, X., White, M.A., Ortega, J., Surtees, J.A., and Alani, E. (2017). The mismatch repair and meiotic recombination endonuclease Mlh1-Mlh3 is activated by polymer formation and can cleave DNA substrates in trans. PLoS biology *15*, e2001164.

Marsolier-Kergoat, M.C., Khan, M.M., Schott, J., Zhu, X., and Llorente, B. (2018). Mechanistic View and Genetic Control of DNA Recombination during Meiosis. Molecular cell *70*, 9-20 e26.

bioRxiv preprint doi: https://doi.org/10.1101/386458; this version posted August 7, 2018. The copyright holder for this preprint (which was not certified by peer review) is the author/funder, who has granted bioRxiv a license to display the preprint in perpetuity. It is made available under aCC-BY-NC-ND 4.0 International license.

Martini, E., Borde, V., Legendre, M., Audic, S., Regnault, B., Soubigou, G., Dujon, B., and Llorente, B. (2011). Genome-wide analysis of heteroduplex DNA in mismatch repair-deficient yeast cells reveals novel properties of meiotic recombination pathways. PLoS genetics *7*, e1002305.

Matos, J., Lipp, J.J., Bogdanova, A., Guillot, S., Okaz, E., Junqueira, M., Shevchenko, A., and Zachariae, W. (2008). Dbf4-dependent CDC7 kinase links DNA replication to the segregation of homologous chromosomes in meiosis I. Cell *135*, 662-678.

Matsumoto, S., and Masai, H. (2013). Regulation of chromosome dynamics by Hsk1/Cdc7 kinase. Biochem Soc Trans *41*, 1712-1719.

Mazina, O.M., Mazin, A.V., Nakagawa, T., Kolodner, R.D., and Kowalczykowski, S.C. (2004). Saccharomyces cerevisiae Mer3 helicase stimulates 3'-5' heteroduplex extension by Rad51; implications for crossover control in meiotic recombination. Cell *117*, 47-56.

Murakami, H., and Keeney, S. (2014). Temporospatial coordination of meiotic DNA replication and recombination via DDK recruitment to replisomes. Cell *158*, 861-873.

Nakagawa, T., and Kolodner, R.D. (2002). Saccharomyces cerevisiae Mer3 is a DNA helicase involved in meiotic crossing over. Molecular and cellular biology *22*, 3281-3291.

Nishant, K.T., Chen, C., Shinohara, M., Shinohara, A., and Alani, E. (2010). Genetic analysis of baker's yeast Msh4-Msh5 reveals a threshold crossover level for meiotic viability. PLoS genetics *6*.

Nishant, K.T., Plys, A.J., and Alani, E. (2008). A mutation in the putative MLH3 endonuclease domain confers a defect in both mismatch repair and meiosis in Saccharomyces cerevisiae. Genetics *179*, 747-755.

Niu, H., Li, X., Job, E., Park, C., Moazed, D., Gygi, S.P., and Hollingsworth, N.M. (2007). Mek1 kinase is regulated to suppress double-strand break repair between sister chromatids during budding yeast meiosis. Molecular and cellular biology *27*, 5456-5467.

bioRxiv preprint doi: https://doi.org/10.1101/386458; this version posted August 7, 2018. The copyright holder for this preprint (which was not certified by peer review) is the author/funder, who has granted bioRxiv a license to display the preprint in perpetuity. It is made available under aCC-BY-NC-ND 4.0 International license.

Niu, H., Wan, L., Baumgartner, B., Schaefer, D., Loidl, J., and Hollingsworth, N.M. (2005). Partner choice during meiosis is regulated by Hop1-promoted dimerization of Mek1. Molecular biology of the cell *16*, 5804-5818.

Niu, H., Wan, L., Busygina, V., Kwon, Y., Allen, J.A., Li, X., Kunz, R.C., Kubota, K., Wang, B., Sung, P.*, et al.* (2009). Regulation of meiotic recombination via Mek1-mediated Rad54 phosphorylation. Molecular cell *36*, 393-404.

Novak, J.E., Ross-Macdonald, P.B., and Roeder, G.S. (2001). The budding yeast Msh4 protein functions in chromosome synapsis and the regulation of crossover distribution. Genetics *158*, 1013-1025.

Oh, S.D., Lao, J.P., Hwang, P.Y., Taylor, A.F., Smith, G.R., and Hunter, N. (2007). BLM ortholog, Sgs1, prevents aberrant crossing-over by suppressing formation of multichromatid joint molecules. Cell *130*, 259-272.

Papazian, H.P. (1952). The analysis of tetrad data. Genetics *37*, 175-188.

Prugar, E., Burnett, C., Chen, X., and Hollingsworth, N.M. (2017). Coordination of Double Strand Break Repair and Meiotic Progression in Yeast by a Mek1-Ndt80 Negative Feedback Loop. Genetics *206*, 497-512.

Qiao, H., Prasada Rao, H.B., Yang, Y., Fong, J.H., Cloutier, J.M., Deacon, D.C., Nagel, K.E., Swartz, R.K., Strong, E., Holloway, J.K.*, et al.* (2014). Antagonistic roles of ubiquitin ligase HEI10 and SUMO ligase RNF212 regulate meiotic recombination. Nature genetics *46*, 194-199.

Rakshambikai, R., Srinivasan, N., and Nishant, K.T. (2013). Structural insights into Saccharomyces cerevisiae Msh4-Msh5 complex function using homology modeling. PloS one *8*, e78753.

Ranjha, L., Anand, R., and Cejka, P. (2014). The Saccharomyces cerevisiae Mlh1-Mlh3 heterodimer is an endonuclease that preferentially binds to Holliday junctions. The Journal of biological chemistry *289*, 5674-5686.

bioRxiv preprint doi: https://doi.org/10.1101/386458; this version posted August 7, 2018. The copyright holder for this preprint (which was not certified by peer review) is the author/funder, who has granted bioRxiv a license to display the preprint in perpetuity. It is made available under aCC-BY-NC-ND 4.0 International license.

Rao, H.B., Qiao, H., Bhatt, S.K., Bailey, L.R., Tran, H.D., Bourne, S.L., Qiu, W., Deshpande, A., Sharma, A.N., Beebout, C.J.*, et al.* (2017). A SUMO-ubiquitin relay recruits proteasomes to chromosome axes to regulate meiotic recombination. Science *355*, 403-407.

Reynolds, A., Qiao, H., Yang, Y., Chen, J.K., Jackson, N., Biswas, K., Holloway, J.K., Baudat, F., de Massy, B., Wang, J.*, et al.* (2013). RNF212 is a dosage-sensitive regulator of crossing-over during mammalian meiosis. Nature genetics *45*, 269-278.

Rockmill, B., Fung, J.C., Branda, S.S., and Roeder, G.S. (2003). The Sgs1 helicase regulates chromosome synapsis and meiotic crossing over. Current biology : CB *13*, 1954-1962.

Rockmill, B., Lefrancois, P., Voelkel-Meiman, K., Oke, A., Roeder, G.S., and Fung, J.C. (2013). High throughput sequencing reveals alterations in the recombination signatures with diminishing Spo11 activity. PLoS genetics *9*, e1003932.

Rogacheva, M.V., Manhart, C.M., Chen, C., Guarne, A., Surtees, J., and Alani, E. (2014). Mlh1-Mlh3, a meiotic crossover and DNA mismatch repair factor, is a Msh2-Msh3-stimulated endonuclease. The Journal of biological chemistry *289*, 5664-5673.

Sasanuma, H., Hirota, K., Fukuda, T., Kakusho, N., Kugou, K., Kawasaki, Y., Shibata, T., Masai, H., and Ohta, K. (2008). Cdc7-dependent phosphorylation of Mer2 facilitates initiation of yeast meiotic recombination. Genes & development *22*, 398-410.

Seoane, A.I., and Morgan, D.O. (2017). Firing of Replication Origins Frees Dbf4-Cdc7 to Target Eco1 for Destruction. Current biology : CB *27*, 2849-2855 e2842.

Shinohara, M., Oh, S.D., Hunter, N., and Shinohara, A. (2008). Crossover assurance and crossover interference are distinctly regulated by the ZMM proteins during yeast meiosis. Nature genetics *40*, 299-309.

Snowden, T., Acharya, S., Butz, C., Berardini, M., and Fishel, R. (2004). hMSH4-hMSH5 recognizes Holliday Junctions and forms a meiosis-specific sliding clamp that embraces homologous chromosomes. Molecular cell *15*, 437-451.

bioRxiv preprint doi: https://doi.org/10.1101/386458; this version posted August 7, 2018. The copyright holder for this preprint (which was not certified by peer review) is the author/funder, who has granted bioRxiv a license to display the preprint in perpetuity. It is made available under aCC-BY-NC-ND 4.0 International license.

Sourirajan, A., and Lichten, M. (2008). Polo-like kinase Cdc5 drives exit from pachytene during budding yeast meiosis. Genes & development *22*, 2627-2632.

Stahl, F.W., Foss, H.M., Young, L.S., Borts, R.H., Abdullah, M.F., and Copenhaver, G.P. (2004). Does crossover interference count in Saccharomyces cerevisiae? Genetics *168*, 35-48.

Subramanian, V.V., MacQueen, A.J., Vader, G., Shinohara, M., Sanchez, A., Borde, V., Shinohara, A., and Hochwagen, A. (2016). Chromosome Synapsis Alleviates Mek1-Dependent Suppression of Meiotic DNA Repair. PLoS biology *14*, e1002369.

Sym, M., Engebrecht, J.A., and Roeder, G.S. (1993). ZIP1 is a synaptonemal complex protein required for meiotic chromosome synapsis. Cell *72*, 365-378.

Sym, M., and Roeder, G.S. (1995). Zip1-induced changes in synaptonemal complex structure and polycomplex assembly. The Journal of cell biology *128*, 455-466.

Tang, S., Wu, M.K., Zhang, R., and Hunter, N. (2015). Pervasive and essential roles of the Top3-Rmi1 decatenase orchestrate recombination and facilitate chromosome segregation in meiosis. Molecular cell *57*, 607-621.

Thacker, D., Mohibullah, N., Zhu, X., and Keeney, S. (2014). Homologue engagement controls meiotic DNA break number and distribution. Nature *510*, 241-246.

Tsubouchi, H., and Roeder, G.S. (2002). The Mnd1 protein forms a complex with hop2 to promote homologous chromosome pairing and meiotic double-strand break repair. Molecular and cellular biology *22*, 3078-3088.

Valentin, G., Schwob, E., and Della Seta, F. (2006). Dual role of the Cdc7-regulatory protein Dbf4 during yeast meiosis. The Journal of biological chemistry *281*, 2828-2834.

Voelkel-Meiman, K., Johnston, C., Thappeta, Y., Subramanian, V.V., Hochwagen, A., and MacQueen, A.J. (2015). Separable Crossover-Promoting and Crossover-Constraining Aspects of Zip1 Activity during Budding Yeast Meiosis. PLoS genetics *11*, e1005335.

bioRxiv preprint doi: https://doi.org/10.1101/386458; this version posted August 7, 2018. The copyright holder for this preprint (which was not certified by peer review) is the author/funder, who has granted bioRxiv a license to display the preprint in perpetuity. It is made available under aCC-BY-NC-ND 4.0 International license.

Wan, L., de los Santos, T., Zhang, C., Shokat, K., and Hollingsworth, N.M. (2004). Mek1 kinase activity functions downstream of RED1 in the regulation of meiotic double strand break repair in budding yeast. Molecular biology of the cell *15*, 11-23.

Wan, L., Niu, H., Futcher, B., Zhang, C., Shokat, K.M., Boulton, S.J., and Hollingsworth, N.M. (2008). Cdc28-Clb5 (CDK-S) and Cdc7-Dbf4 (DDK) collaborate to initiate meiotic recombination in yeast. Genes & development *22*, 386-397.

Wan, L., Zhang, C., Shokat, K.M., and Hollingsworth, N.M. (2006). Chemical inactivation of cdc7 kinase in budding yeast results in a reversible arrest that allows efficient cell synchronization prior to meiotic recombination. Genetics *174*, 1767-1774.

Wang, K., Wang, M., Tang, D., Shen, Y., Miao, C., Hu, Q., Lu, T., and Cheng, Z. (2012). The role of rice HEI10 in the formation of meiotic crossovers. PLoS genetics *8*, e1002809.

Wang, S., Hassold, T., Hunt, P., White, M.A., Zickler, D., Kleckner, N., and Zhang, L. (2017). Inefficient Crossover Maturation Underlies Elevated Aneuploidy in Human Female Meiosis. Cell *168*, 977-989 e917.

Watanabe, Y. (2012). Geometry and force behind kinetochore orientation: lessons from meiosis. Nature reviews Molecular cell biology *13*, 370-382.

Wijnker, E., Velikkakam James, G., Ding, J., Becker, F., Klasen, J.R., Rawat, V., Rowan, B.A., de Jong, D.F., de Snoo, C.B., Zapata, L.*, et al.* (2013). The genomic landscape of meiotic crossovers and gene conversions in Arabidopsis thaliana. eLife *2*, e01426.

Woglar, A., and Villeneuve, A.M. (2018). Dynamic Architecture of DNA Repair Complexes and the Synaptonemal Complex at Sites of Meiotic Recombination. Cell *173*, 1678-1691 e1616.

Wu, H.Y., Ho, H.C., and Burgess, S.M. (2010). Mek1 kinase governs outcomes of meiotic recombination and the checkpoint response. Current biology : CB *20*, 1707-1716.

Yang, W., Junop, M.S., Ban, C., Obmolova, G., and Hsieh, P. (2000). DNA mismatch repair: from structure to mechanism. Cold Spring Harb Symp Quant Biol *65*, 225-232.

bioRxiv preprint doi: https://doi.org/10.1101/386458; this version posted August 7, 2018. The copyright holder for this preprint (which was not certified by peer review) is the author/funder, who has granted bioRxiv a license to display the preprint in perpetuity. It is made available under aCC-BY-NC-ND 4.0 International license.

Yokoo, R., Zawadzki, K.A., Nabeshima, K., Drake, M., Arur, S., and Villeneuve, A.M. (2012). COSA-1 reveals robust homeostasis and separable licensing and reinforcement steps governing meiotic crossovers. Cell *149*, 75-87.

Zakharyevich, K., Ma, Y., Tang, S., Hwang, P.Y., Boiteux, S., and Hunter, N. (2010). Temporally and biochemically distinct activities of Exo1 during meiosis: double-strand break resection and resolution of double Holliday junctions. Molecular cell *40*, 1001-1015.

Zakharyevich, K., Tang, S., Ma, Y., and Hunter, N. (2012). Delineation of joint molecule resolution pathways in meiosis identifies a crossover-specific resolvase. Cell *149*, 334-347.

Zhang, L., Kohler, S., Rillo-Bohn, R., and Dernburg, A.F. (2018). A compartmentalized signaling network mediates crossover control in meiosis. eLife *7*.

Zhang, L., Tang, D., Luo, Q., Chen, X., Wang, H., Li, Y., and Cheng, Z. (2014). Crossover formation during rice meiosis relies on interaction of OsMSH4 and OsMSH5. Genetics *198*, 1447-1456.

Zickler, D., and Kleckner, N. (2015). Recombination, Pairing, and Synapsis of Homologs during Meiosis. Cold Spring Harbor perspectives in biology *7*.

bioRxiv preprint doi: https://doi.org/10.1101/386458; this version posted August 7, 2018. The copyright holder for this preprint (which was not certified by peer review) is the author/funder, who has granted bioRxiv a license to display the preprint in perpetuity. It is made available under aCC-BY-NC-ND 4.0 International license.

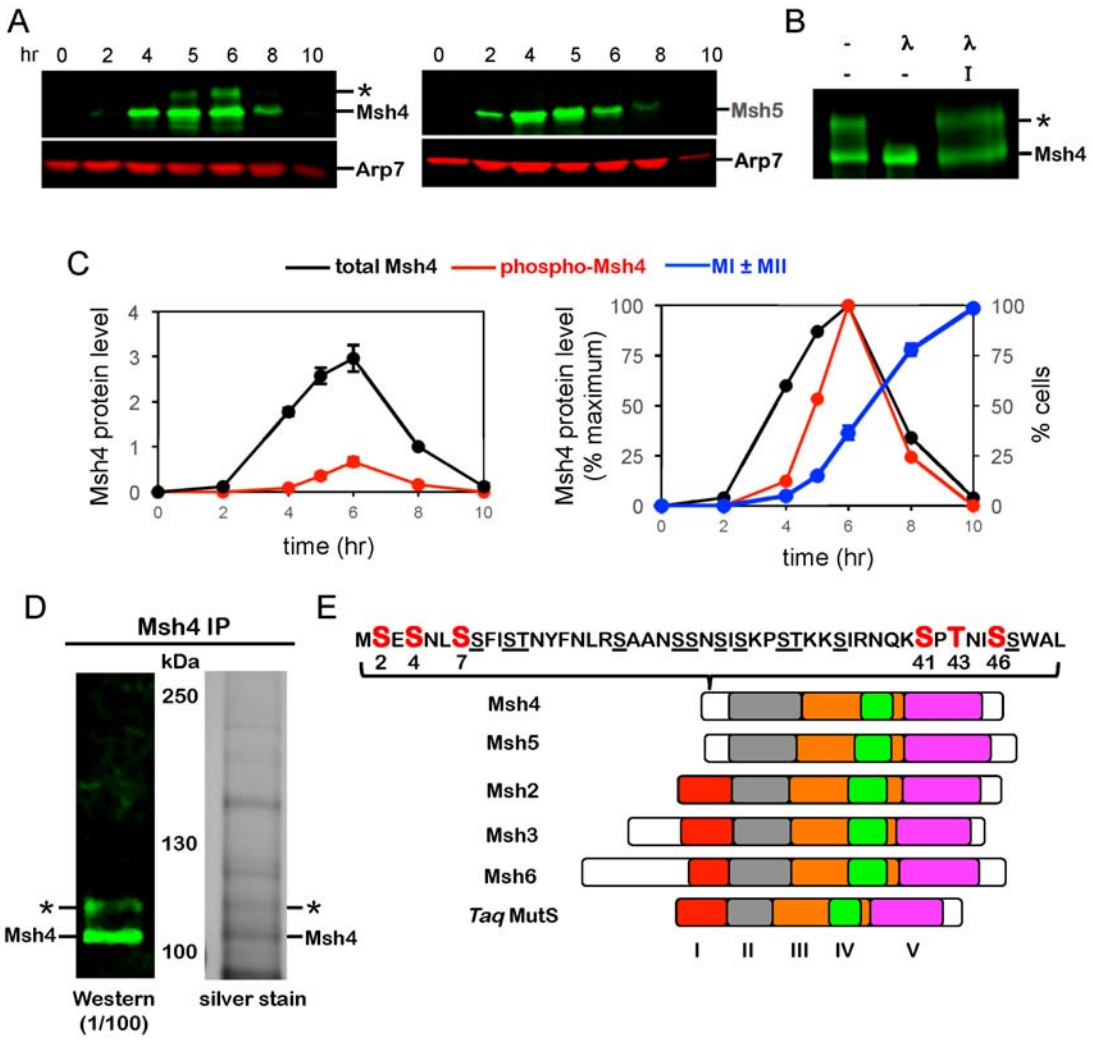

Figure 1. The N-terminal region of Msh4 is phosphorylated.

(A) Western analysis of Msh4 (left) and Msh5 (right) throughout meiosis. Asterisk indicates modified Msh4. Arp7 is used throughout as a loading control (Sourirajan and Lichten, 2008).

(B) Lambda phosphatase treatment of immuno-precipitated Msh4. λ, phosphatase inhibitor; I, phosphatase inhibitor.

(C) Relative (left) and normalized (right) levels Msh4 phosphorylation. MI ± MII is the percentage of cells that have completed one or both meiotic divisions. Error bars show mean ± S.E. from four independent time courses.

bioRxiv preprint doi: https://doi.org/10.1101/386458; this version posted August 7, 2018. The copyright holder for this preprint (which was not certified by peer review) is the author/funder, who has granted bioRxiv a license to display the preprint in perpetuity. It is made available under aCC-BY-NC-ND 4.0 International license.

(D) Western blotting and silver-stained gel images of immuno-precipitated material used for LC-MS/MS analysis. The positions of modified and unmodified Msh4 bands that were excised and processed for LC-MS/MS are indicated.

(E) Positions of phosphorylation sites (red) mapped by LC-MS/MS. Underlined residues highlight the high S/T content of the Msh4 N-terminal region. Diagrams show protein domains of eukaryotic nuclear MutS homologs relative to *Thermus aquaticus* MutS (adapted from (Nishant et al., 2010). Also see **Figure S1**.

bioRxiv preprint doi: https://doi.org/10.1101/386458; this version posted August 7, 2018. The copyright holder for this preprint (which was not certified by peer review) is the author/funder, who has granted bioRxiv a license to display the preprint in perpetuity. It is made available under aCC-BY-NC-ND 4.0 International license.

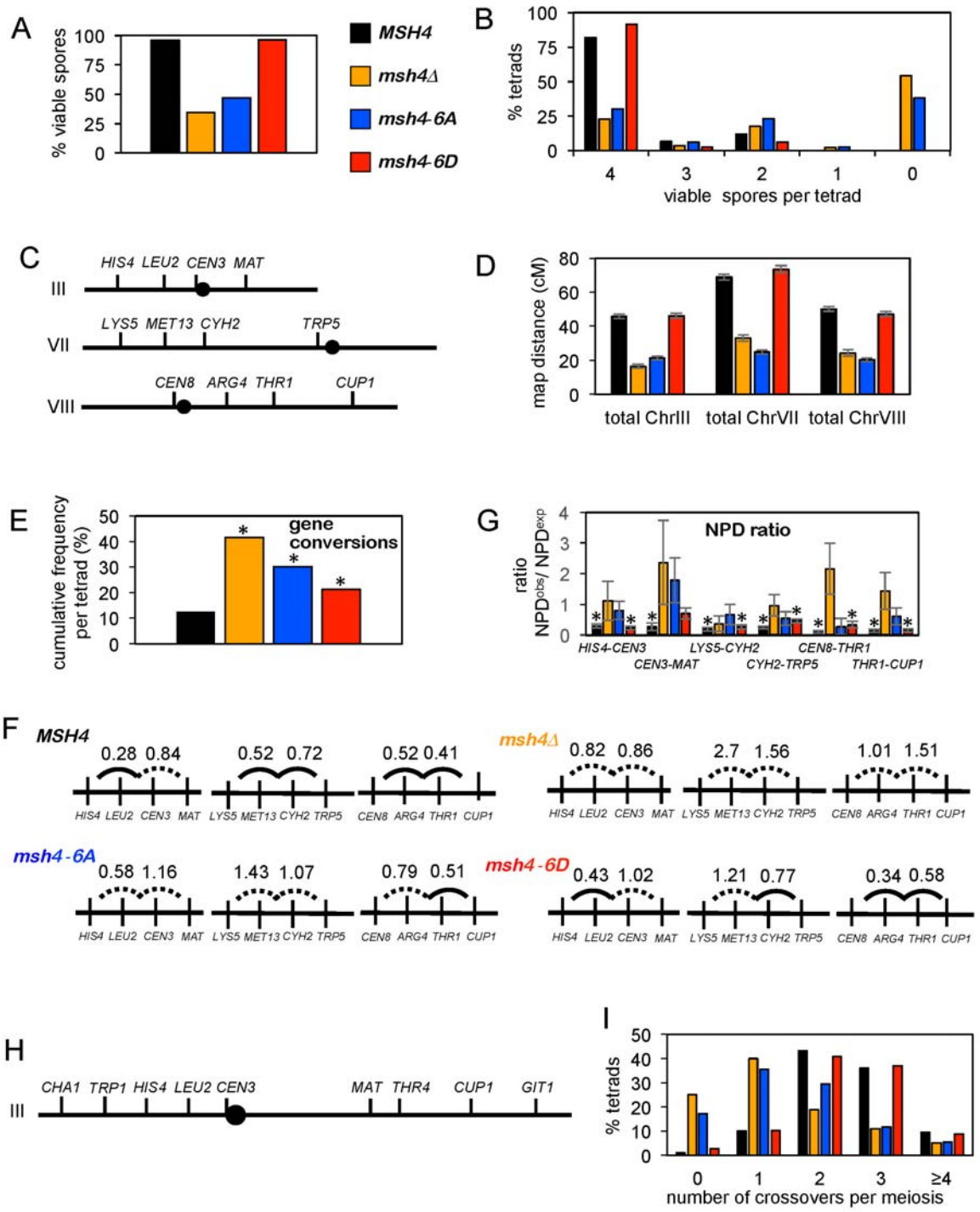

Figure 2. Phosphorylation is essential for the crossover function of Msh4.

(A) Spore viabilities of indicated strains (see **Table S1**).

(B). Distributions of tetrads with 4, 3, 2, 1 and 0 viable spores.

bioRxiv preprint doi: https://doi.org/10.1101/386458; this version posted August 7, 2018. The copyright holder for this preprint (which was not certified by peer review) is the author/funder, who has granted bioRxiv a license to display the preprint in perpetuity. It is made available under aCC-BY-NC-ND 4.0 International license.

(C) Marker configurations in strains used to analyze recombination. *CEN3* is marked with the *ADE2* gene and *CEN8* is marked with *URA3* (Oh et al., 2007).

(D) Cumulative map distances (± S.E.) for intervals on chromosomes III, VII and VIII (see **Table S2**).

(E) Cumulative frequencies of tetrads with gene conversions (non 2:2 segregations) for markers shown in (E). Asterisks indicate $P<0.01$ relative to wild type (*z*-test).

(F) Interference analysis for adjacent intervals (Lao et al., 2013; Malkova et al., 2004). Solid arcs between intervals indicate significant positive interference; failure to detect significant positive interference is indicated by dashed arcs (see **Table S3**).

(G) Interference analysis within individual intervals expressed as NPD ratios (https://elizabethhousworth.com/StahlLabOnlineTools/). Error bars show S.E. Asterisks indicate significant positive interference (see **Table S4**).

(H) Marker configuration in strains used to analyze crossover assurance for chromosome III. *CEN3* is heterozgously marked with the *LYS2 and URA3***.**

(I) Distributions of crossover classes for chromosome III (see **Table S5**).

See also **Figures S2** and **S3**.

bioRxiv preprint doi: https://doi.org/10.1101/386458; this version posted August 7, 2018. The copyright holder for this preprint (which was not certified by peer review) is the author/funder, who has granted bioRxiv a license to display the preprint in perpetuity. It is made available under aCC-BY-NC-ND 4.0 International license.

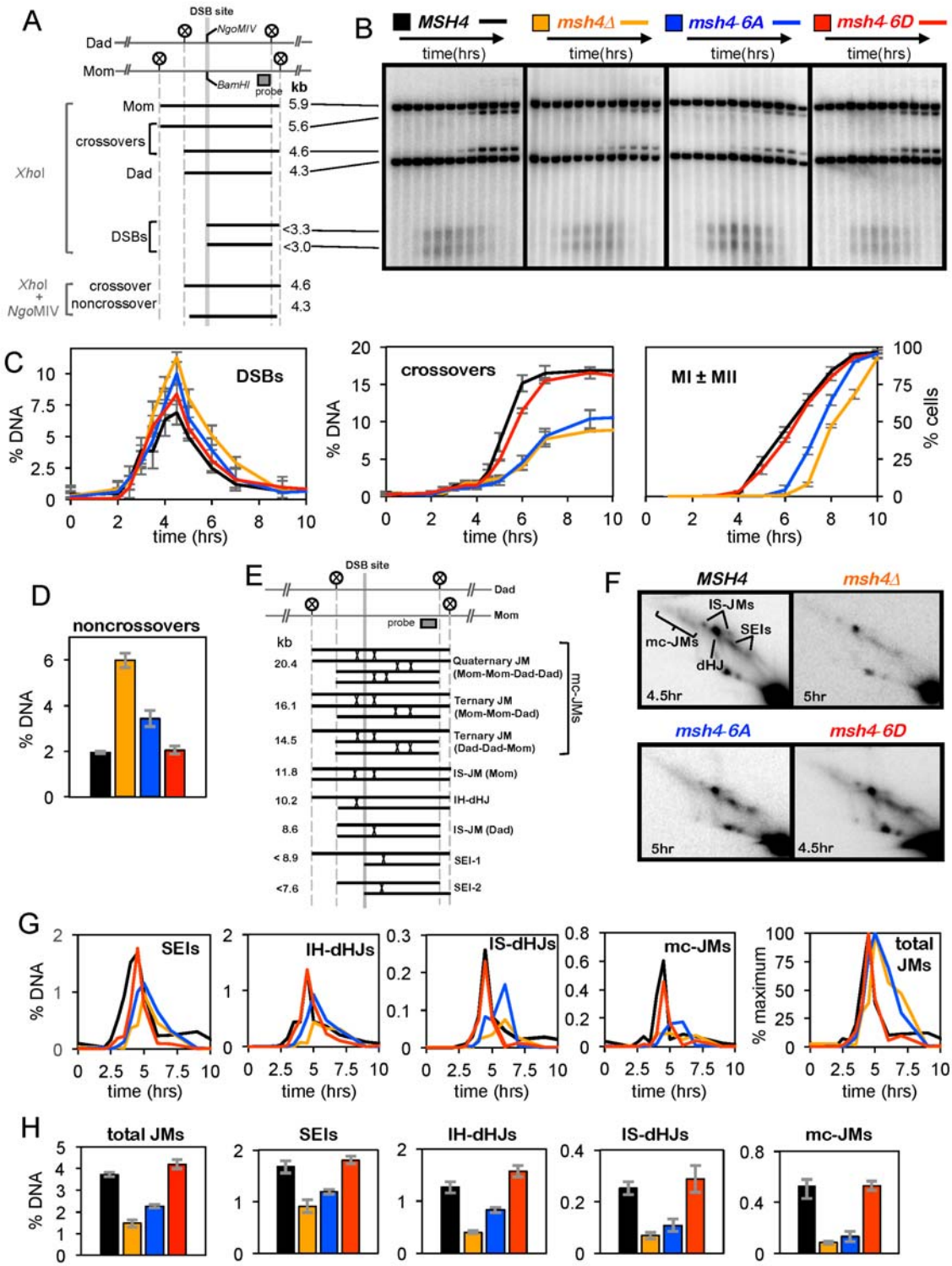

Figure 3. Physical analysis of the DNA events of meiotic recombination.

(A) Map of *HIS4:LEU2* locus highlighting the DSB site, *Xho*I restriction sites (circled Xs) and the position of the probe used in Southern blotting. Sizes of diagnostic fragments are shown below.

bioRxiv preprint doi: https://doi.org/10.1101/386458; this version posted August 7, 2018. The copyright holder for this preprint (which was not certified by peer review) is the author/funder, who has granted bioRxiv a license to display the preprint in perpetuity. It is made available under aCC-BY-NC-ND 4.0 International license.

(B) Representative 1D gel Southern blot images for analysis of DSBs and crossovers. Time points are 0, 2, 2.5, 3, 3.5, 4, 4.5, 5, 6, 7, 9 and 11 hours.

(C) Quantification of DSBs, crossovers and meiotic divisions. %DNA is percentage of total hybridizing DNA signal. MI ± MII is the percentage of cells that have completed one or both meiotic divisions.

(D) Non-crossover levels at 11 hrs.

(E) JM structures detected at the *HIS4:LEU2* locus. Positions of the DSB site, diagnostic *Xho*I sites (circled Xs) and the Southern probe are shown.

(F) Representative 2D gel Southern blot images for time points where JM levels peak. Positions of the various JM signals are indicated in the first panel.

(G) Quantification of JM species over time. (H) Quantification of JM species at their peak levels from three independent time courses. IH-dHJs, inter-homolog dHJs; IS-JMs, intersister JMs (most likely dHJs); SEIs, single-end invasions; mcJMs, multi-chromatid JMs) and total JMs are indicated. Averages ± S.E. were calculated from three independent experiments.

bioRxiv preprint doi: https://doi.org/10.1101/386458; this version posted August 7, 2018. The copyright holder for this preprint (which was not certified by peer review) is the author/funder, who has granted bioRxiv a license to display the preprint in perpetuity. It is made available under aCC-BY-NC-ND 4.0 International license.

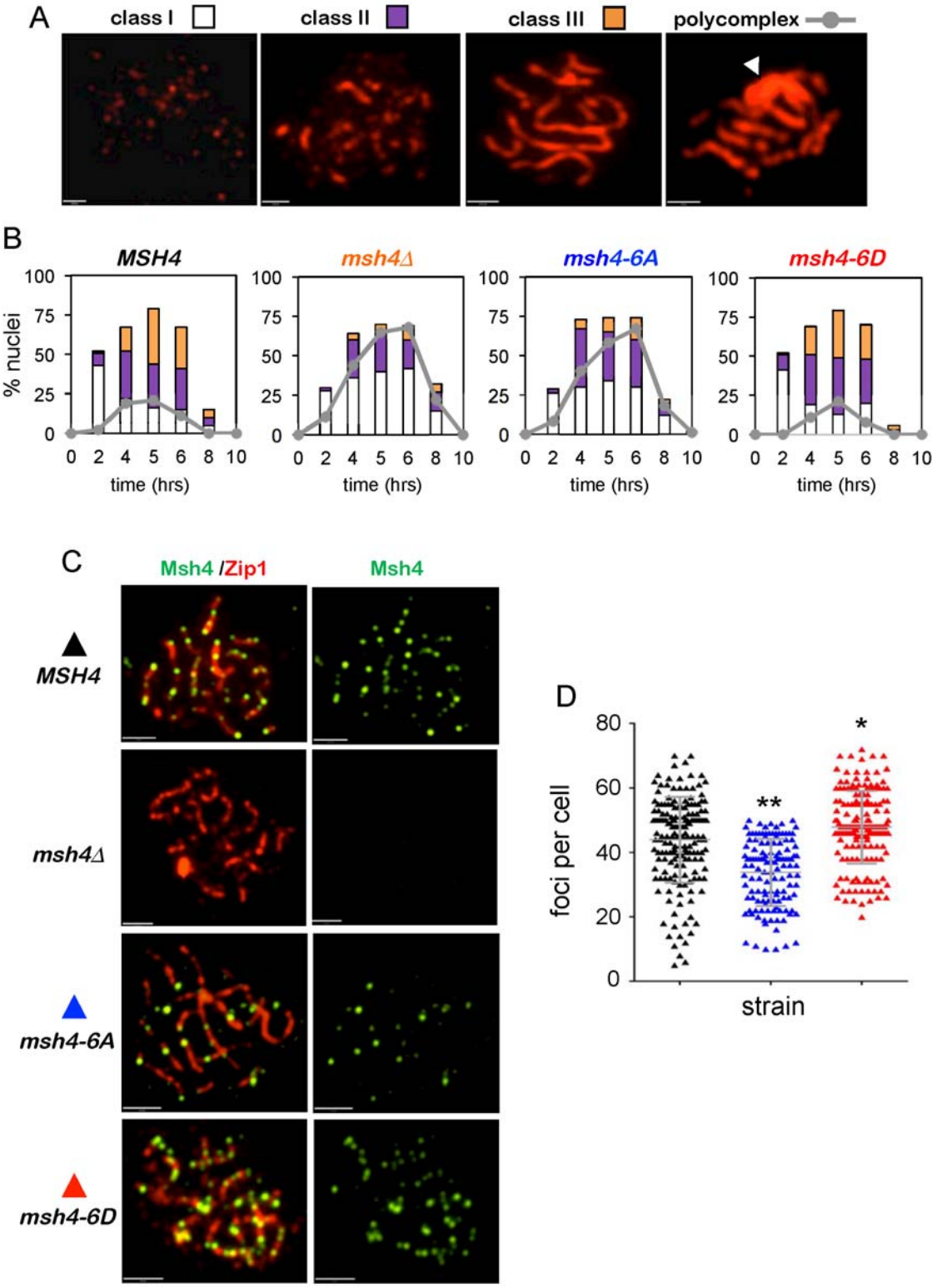

Figure 4. Chromosome synapsis and localization of MutSγ are facilitated by Msh4 phosphorylation.

bioRxiv preprint doi: https://doi.org/10.1101/386458; this version posted August 7, 2018. The copyright holder for this preprint (which was not certified by peer review) is the author/funder, who has granted bioRxiv a license to display the preprint in perpetuity. It is made available under aCC-BY-NC-ND 4.0 International license.

(A) Chromosome spreads showing representative examples of the three different Zip1 immuno-staining classes and a Zip1 polycomplex.

(B) Quantification of Zip1 staining classes and polycomplexes. ≥100 nuclei were scored for each time point.

(C) Representative images of spread meiotic nuclei immuno-stained for Msh4 (green) and Zip1 (red).

(D) Quantification of Msh4 immuno-staining foci in class II and class III nuclei. ≥100 nuclei were scored for each strain. *P<0.05; **P<0.01 two tailed Mann Whitney test. Scale bars = 30 μm.

Also see **Figure S4**.

bioRxiv preprint doi: https://doi.org/10.1101/386458; this version posted August 7, 2018. The copyright holder for this preprint (which was not certified by peer review) is the author/funder, who has granted bioRxiv a license to display the preprint in perpetuity. It is made available under aCC-BY-NC-ND 4.0 International license.

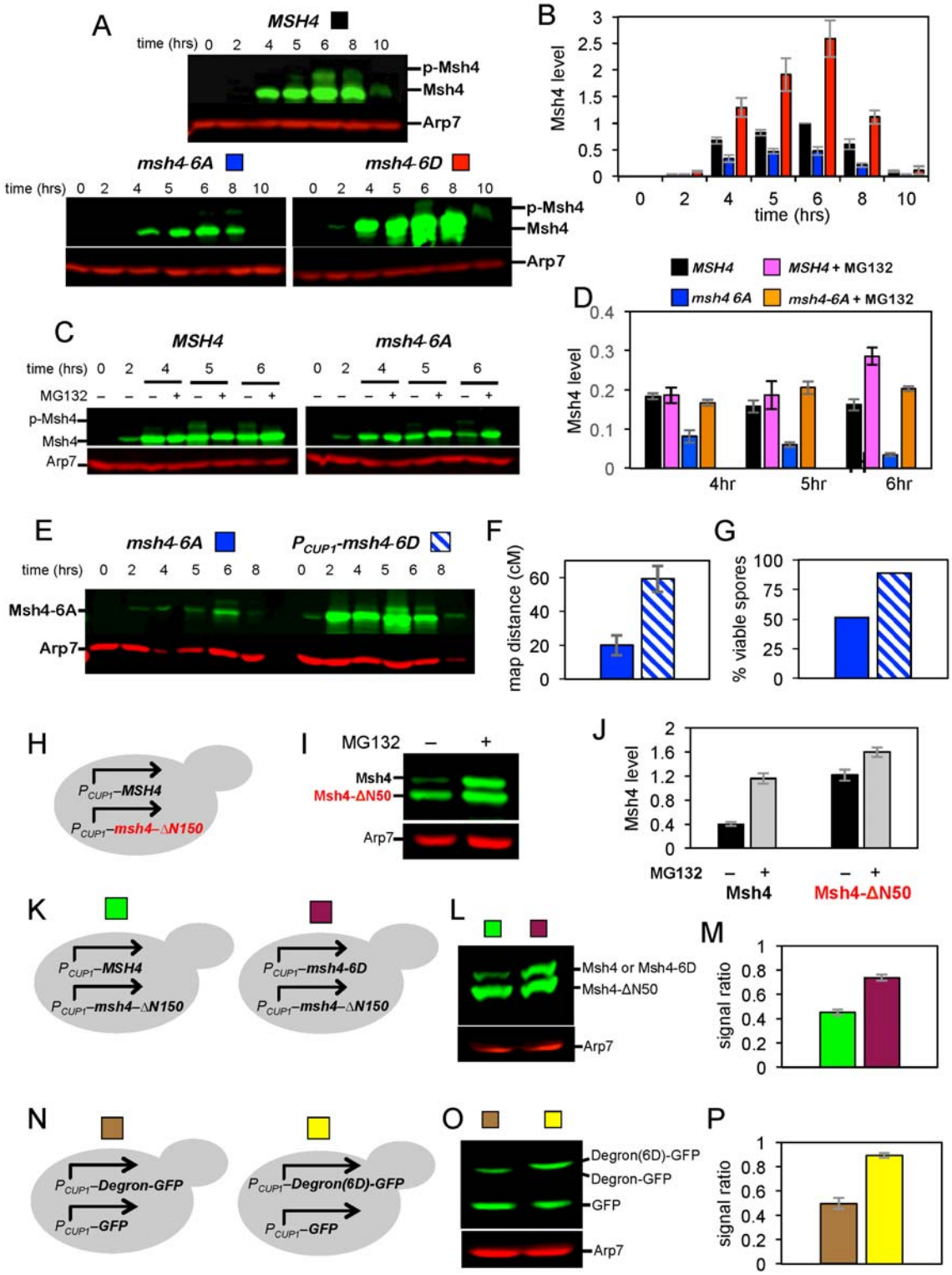

Figure 5. Degron activity of the Msh4 N-terminal region is attenuated by phosphorylation

(A) Western analysis of Msh4 during meiosis in wild-type, *msh-6A* and *msh4-6D* strains.

bioRxiv preprint doi: https://doi.org/10.1101/386458; this version posted August 7, 2018. The copyright holder for this preprint (which was not certified by peer review) is the author/funder, who has granted bioRxiv a license to display the preprint in perpetuity. It is made available under aCC-BY-NC-ND 4.0 International license.

(B) Quantification of Msh4 protein relative to the Arp7 loading control. Averages ± S.E. were calculated from three independent experiments (also see **Figure S5**).

(C) Western analysis of Msh4 with and without addition of the proteasome inhibitor, MG132, at 2 hrs.

(D) Quantification of Msh4 protein with and without MG132 treatment. Averages ± S.E. calculated from three independent experiments.

(E) Western analysis of msh4-6A protein during meiosis in the *msh4-6A* strain and following copper-induced overexpression in a P_{CUP1}-*msh4-6A* strain.

(F) Spore viability of *msh4-6A* and P_{CUP1}-*msh4-6A* strains.

(G) Map distances (± S.E.) for intervals flanking the *HIS4::LEU2* recombination hotspot (see **Figure S3**) in tetrads from *msh4-6A* and P_{CUP1}-*msh4-6A* strains.

(H) Experimental system for copper-inducible expression of Msh4 and msh4-ΔN50 proteins in vegetative cells.

(I) Western analysis of the stains shown in panel E following copper induction, with and without MG132 treatment.

(J) Quantification of the experiments represented in panels D and E. Averages ± S.E. were calculated from four independent experiments (also see **Figures S5** and **S6**).

(K) Experimental systems for co-expression of Msh4 and Msh4-ΔN50 (left), or Msh4-6D and Msh4-ΔN50 proteins (right).

(L) Western analysis of the stains shown in panel H following copper induction, with and without MG132 treatment.

(M) Quantification of experiments represented in panels H and I. Average ratios ± S.E. were calculated from four independent experiments (also see **Figure S5**).

(N) Experimental systems for co-expression of GFP and the Msh4 N-terminal region ("degron") fused to GFP (left); or co-expresson of GFP and a phospho-mimetic derivative of the Msh4 N-terminal region ("degron 6D) fused to GFP.

bioRxiv preprint doi: https://doi.org/10.1101/386458; this version posted August 7, 2018. The copyright holder for this preprint (which was not certified by peer review) is the author/funder, who has granted bioRxiv a license to display the preprint in perpetuity. It is made available under aCC-BY-NC-ND 4.0 International license.

(O) Western analysis of the stains shown in panel K following copper induction.

(P) Quantification of experiments represented in panels K and L. Average ratios ± S.E. were calculated from four independent experiments (also see **Figure S5**).

bioRxiv preprint doi: https://doi.org/10.1101/386458; this version posted August 7, 2018. The copyright holder for this preprint (which was not certified by peer review) is the author/funder, who has granted bioRxiv a license to display the preprint in perpetuity. It is made available under aCC-BY-NC-ND 4.0 International license.

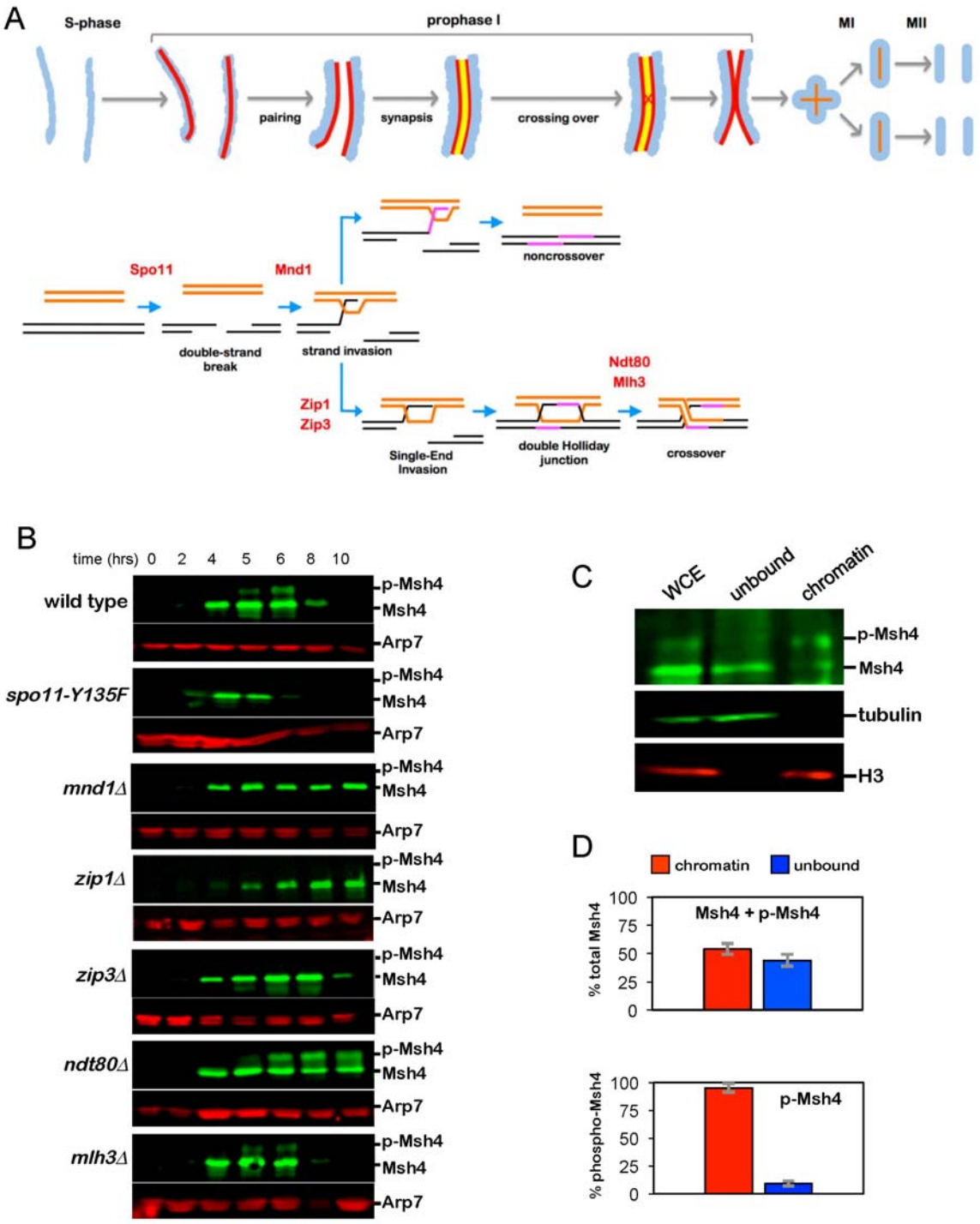

Figure 6. Genetic requirements and chromatin association of phosphorylated of Msh4.

(A) Chromosomal and recombination events of meiosis illustrating the steps affected by mutants analyzed in panel B. Blue, chromatin; red lines, homolog axes; yellow line, synaptonemal complex central region.

bioRxiv preprint doi: https://doi.org/10.1101/386458; this version posted August 7, 2018. The copyright holder for this preprint (which was not certified by peer review) is the author/funder, who has granted bioRxiv a license to display the preprint in perpetuity. It is made available under aCC-BY-NC-ND 4.0 International license.

(B) Western analysis of Msh4 in the indicated mutants.

(C) Western analysis Msh4 in whole cell extracts ("WCE") and extracts separated into soluble ("unbound") and chromatin fractions. Tubulin and histone H3 are markers for these two fractions. (D) Quantification of total Msh4 (top graph) and phosphorylated Msh4 (bottom graph) in the two fractions. Means values ±S.E. were calculated from three independent experiments.

bioRxiv preprint doi: https://doi.org/10.1101/386458; this version posted August 7, 2018. The copyright holder for this preprint (which was not certified by peer review) is the author/funder, who has granted bioRxiv a license to display the preprint in perpetuity. It is made available under aCC-BY-NC-ND 4.0 International license.

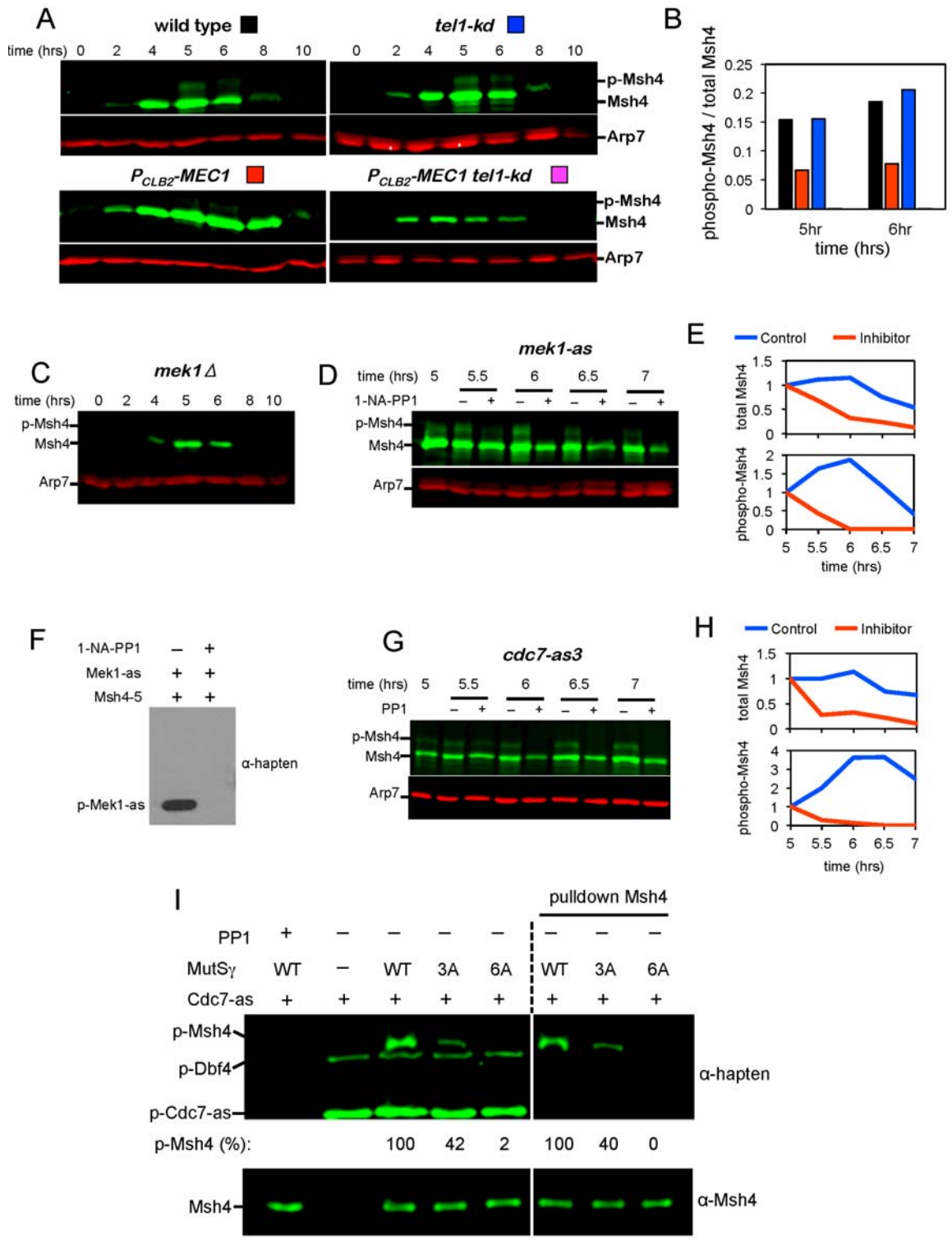

Figure 7. Kinase requirements for phosphorylation of Msh4 *in vivo* and *in vitro*.

(A) Western analysis of Msh4 in *tel1-kd*, *pCLB2-MEC1* and *pCLB2-MEC1 tel1-kd* strains during meiosis.

bioRxiv preprint doi: https://doi.org/10.1101/386458; this version posted August 7, 2018. The copyright holder for this preprint (which was not certified by peer review) is the author/funder, who has granted bioRxiv a license to display the preprint in perpetuity. It is made available under aCC-BY-NC-ND 4.0 International license.

(B) Fraction of Msh4 that is phosphorylated at 5 and 6 hrs in the experiments shown in panel (A).

(C) Western analysis of Msh4 in a *mek1*Δ null mutant.

(D) Western analysis of Msh4 in strains containing the ATP-analog sensitive *mek1-as* allele, with and without addition of the inhibitor 1-NA-PP1 at 5 hrs.

(E) Relative levels of total and phosphorylated Msh4 quantified from the experiment shown in panel (D). Levels were normalized to the 5 hr time point.

(F) Western analysis of a Mek1-as *in vitro* kinase assay with MutSg, with and without the inhibitor 1-NA-PP1.

(G) Western analysis of Msh4 in strains containing the ATP-analog sensitive *cdc7-as3* allele, with and without addition of the inhibitor PP1 at 5 hrs. The a-hapten antibody recognizes phosphorylation products of the semi-synthetic epitope system.

(H) Relative levels of total and phosphorylated Msh4 quantified from the experiment shown in panel (G). Levels were normalized to the 5 hrs timepoint.

(I) Western analysis of an *in vitro* kinase assay with the Cdc7-as3 kinase (Cdc7-as3–Dbf4 complex) with wild-type MutSg or mutant derivatives containing serine-alanine substitutions in the N-terminus of Msh4. In the right-hand panel, Msh4 was purified from the reactions. Phosphorylation efficiency was calculated relative to wild-type Msh4. In the lower panels, 10% of each reaction was probed for Msh4 as a loading control. Also see **Figure S7**.